Cell Division Protein FtsZ Is Unfolded for N-Terminal Degradation by Antibiotic-Activated ClpP

Nadine Silber,[a] Stefan Pan,[a] Sina Schäkermann,[b] Christian Mayer,[a] Heike Brötz-Oesterhelt,[a,c] (ID) Peter Sass[a,c]

[a]Department of Microbial Bioactive Compounds, Interfaculty Institute of Microbiology and Infection Medicine, University of Tuebingen, Tuebingen, Germany
[b]Applied Microbiology, Ruhr University Bochum, Bochum, Germany
[c]Cluster of Excellence-Controlling Microbes to Fight Infections, Tuebingen, Germany

Heike Brötz-Oesterhelt and Peter Sass share senior authorship.

ABSTRACT Antibiotic acyldepsipeptides (ADEPs) deregulate ClpP, the proteolytic core of the bacterial Clp protease, thereby inhibiting its native functions and concomitantly activating it for uncontrolled proteolysis of nonnative substrates. Importantly, although ADEP-activated ClpP is assumed to target multiple polypeptide and protein substrates in the bacterial cell, not all proteins seem equally susceptible. In *Bacillus subtilis*, the cell division protein FtsZ emerged to be particularly sensitive to degradation by ADEP-activated ClpP at low inhibitory ADEP concentrations. In fact, FtsZ is the only bacterial protein that has been confirmed to be degraded *in vitro* as well as within bacterial cells so far. However, the molecular reason for this preferred degradation remained elusive. Here, we report the unexpected finding that ADEP-activated ClpP alone, in the absence of any Clp-ATPase, leads to an unfolding and subsequent degradation of the N-terminal domain of FtsZ, which can be prevented by the stabilization of the FtsZ fold via nucleotide binding. At elevated antibiotic concentrations, importantly, the C terminus of FtsZ is notably targeted for degradation in addition to the N terminus. Our results show that different target structures are more or less accessible to ClpP, depending on the ADEP level present. Moreover, our data assign a Clp-ATPase-independent protein unfolding capability to the ClpP core of the bacterial Clp protease and suggest that the protein fold of FtsZ may be more flexible than previously anticipated.

IMPORTANCE Acyldepsipeptide (ADEP) antibiotics effectively kill multidrug-resistant Gram-positive pathogens, including vancomycin-resistant enterococcus, penicillin-resistant *Streptococcus pneumoniae* (PRSP), and methicillin-resistant *Staphylococcus aureus* (MRSA). The antibacterial activity of ADEP depends on a new mechanism of action, i.e., the deregulation of bacterial protease ClpP that leads to bacterial self-digestion. Our data allow new insights into the mode of ADEP action by providing a molecular explanation for the distinct bacterial phenotypes observed at low versus high ADEP concentrations. In addition, we show that ClpP alone, in the absence of any unfoldase or energy-consuming system, and only activated by the small molecule antibiotic ADEP, leads to the unfolding of the cell division protein FtsZ.

KEYWORDS ADEP, antibiotics, acyldepsipeptides, guanosine nucleotides, protein unfolding, cytokinesis, Clp protease, Clp-ATPases

Antibiotic acyldepsipeptides (ADEPs) kill Gram-positive bacteria, including human pathogens, by deregulating the bacterial protease Clp (1–4). The Clp protease is conserved across most bacterial species, where it is naturally involved in protein homeostasis and regulatory proteolysis. Clp is important for maintaining vital cellular functions particularly under stress conditions and directs developmen-

tal processes like cell differentiation, genetic competence, and virulence (5, 6). Thus, Clp protease has emerged as a novel target for antibiotic action and virulence inhibition (7–9).

Clp protease constitutes a macromolecular complex that is composed of a proteolytic core, ClpP, that associates with specific hexameric unfoldases, the Clp-ATPases, and accessory adaptor proteins (8, 10). ClpP forms a tetradecameric, barrel-shaped structure with the proteolytic chamber secluded within the assembled complex. The cognate Clp-ATPases interact with the ClpP tetradecamer via distinct hydrophobic pockets at both sides of the barrel (11). Substrate access to the proteolytic chamber is strictly controlled by the partner Clp-ATPases, which recognize the respective protein substrates, unfold them in an ATP-dependent manner, and thread the unfolded polypeptide chains through the apical and distal entrance pores of the ClpP barrel (12). It is important to note that ClpP is capable of degrading peptides on its own, but not fully folded proteins, and strictly depends on ATP-driven Clp-ATPases for proteolytic activation in the natural context (10, 12).

ADEP antibiotics compete with the Clp-ATPases for the same binding sites on ClpP, which results in a dual mechanism of action; by binding to the hydrophobic pockets of ClpP, ADEPs abrogate the interaction of ClpP with its partner Clp-ATPases, thereby preventing all cellular functions of Clp in general and regulatory proteolysis (13). This is sufficient to kill mycobacteria (14, 15), which rely on a functional Clp system for viability (16). However, in most bacterial species, including *Bacillus subtilis* or *Staphylococcus aureus*, Clp is not essential for growth, and thus, mere Clp inhibition is not sufficient to kill bacteria under normal growth conditions. In such species, a ClpP activation mechanism leads to bacterial killing; ADEP binding supports the oligomerization process of ClpP (13) and locks the catalytic triads in an active conformation via allosteric conformational control (17, 18). ADEP additionally triggers a closed- to open-gate structural transition of the N-terminal segments of ClpP that opens the substrate entrance pore to the proteolytic chamber (19, 20), which is otherwise tightly closed (21). As a result, nonnative polypeptides and protein substrates are now allowed to enter the proteolytic chamber of ClpP and are subsequently degraded in a Clp-ATPase-independent manner (1, 13).

Depending on the applied ADEP concentration, treated bacteria show distinct phenotypes. At high ADEP concentrations, several times the MIC, cells rapidly stop growing due to ceased biomass production (22, 23). This phenotype may be readily explained by the broad destructive capacity of ClpP activation, and we showed earlier that ADEP activates ClpP to degrade nascent protein chains during translation (13), likely causing a depletion of several essential bacterial proteins. In contrast, at concentrations very close to the MIC, ADEP exposure results in a more specific phenotype, namely, bacterial cells retain considerable biosynthetic capacity, with macromolecular syntheses and biomass production proceeding for hours (22). However, cell size significantly increases, as indicated by the swelling of coccoid *S. aureus* and *Streptococcus pneumoniae* cells as well as an impressive filamentation of rod-shaped *B. subtilis*, eventually leading to cell death (22, 23). A strong ongoing biosynthetic capacity with blocked cytokinesis points to a preferential proteolytic target in bacterial cell division, and we reported earlier that this is due to the untimely degradation of the essential cell division protein FtsZ by ADEP-activated ClpP (22). This prominent phenotype clearly distinguishes FtsZ as being particularly susceptible to ADEP-ClpP. Intriguingly, the *B. subtilis* FtsZ protein was completely and easily degraded by ADEP-ClpP *in vitro*, while several other folded proteins were not (22). In exploring this enigma, it emerged that the short, hydrophobic N terminus of *B. subtilis* FtsZ is particularly prone to be targeted by ADEP-ClpP, leading to the unfolding of the FtsZ protein over the course of the degradation process, while degradation of the extended and flexible C terminus of FtsZ is only triggered at increased ADEP concentration. Thereby, our results allow new insight into the stability of the FtsZ protein, suggest extending the mechanistic capabilities of ADEP-ClpP toward ATP-independent protein unfolding, and provide a

molecular explanation for the different bacterial phenotypes observed at low versus high ADEP concentrations.

RESULTS

ADEP-activated ClpP preferentially targets the short N terminus of FtsZ. In this study, we set out to determine the molecular basis for the observed sensitivity of *B. subtilis* FtsZ toward ADEP-ClpP. To validate FtsZ as a preferred target for ADEP-ClpP, we first compared the abundance of the fructose-bisphosphate aldolase (FbaA) in relation to FtsZ in *B. subtilis* and *S. aureus* cells that were exposed to ADEP concentrations close to the MIC ($2\times$ to $3\times$ MIC, i.e., 0.25 μg/ml ADEP2 for *B. subtilis* 168 and 1 μg/ml ADEP2 for *S. aureus* NCTC 8325) (Fig. 1A). Fragments of FbaA (as well as of elongation factor Tu [EF-Tu] and pyruvate kinase [Pyk]) were detected in notable amounts in a previous proteomics study of *S. aureus* cells exposed to ADEP at elevated concentrations ($10\times$ MIC) for an extended time period (3). Therefore, FbaA was assumed to be a target for ADEP-activated ClpP in this previous study. Using immunodetection of FtsZ and FbaA proteins, our results confirmed the rapid and complete degradation of FtsZ after 120 min in ADEP-treated cells; however, the protein concentration of FbaA remained unaltered under these conditions (Fig. 1A). To study this aspect in more detail, we proceeded to test the degradation of *B. subtilis* FbaA, EF-Tu, and Pyk (BsFbaA, BsEF-Tu, and BsPyk, respectively) by ADEP-ClpP using purified proteins *in vitro*. Here, BsFbaA, BsEF-Tu, BsPyk were not notably degraded by ADEP-ClpP under the same conditions *in vitro*, in contrast to FtsZ (Fig. 1B), thereby clearly corroborating a preferential degradation of FtsZ by ADEP-ClpP.

Next, we looked into the published crystal structure of FtsZ to identify structural features that may be potentially prone to degradation. *B. subtilis* FtsZ (BsFtsZ; Protein Data Bank entry 2RHO) (Fig. 1C) comprises an overall globular core protein with two independently folding domains (24–26), the N-terminal and the C-terminal domain, which are connected via the central core helix H7 followed by the T7 loop. The N-terminal domain harbors the nucleotide binding site which interacts with the T7 loop of a second FtsZ monomer to form the GTPase catalytic site (27). The long flexible C terminus (amino acids 316 to 382), which contains the interaction interface for other cell division proteins, as well as the short N terminus (amino acids 1 to 10), are not resolved in the crystal structure due to their inherent flexibility. *In silico* disorder predictions visualized the overall structural disorder of the C terminus (Fig. 1D), making it a structural feature likely to be attacked by ADEP-ClpP, as this flexible amino acid tail may easily diffuse through the opened entrance pores into the degradation chamber of ADEP-ClpP. To test this hypothesis, we constructed several mutant proteins of BsFtsZ and tested them in *in vitro* ADEP-ClpP degradation assays (Fig. 1E and F; see Fig. S1 in the supplemental material). Surprisingly, FtsZ mutants with deleted C termini, either short truncations omitting the last 18 amino acids containing the interaction interface (BsFtsZ$_{1-364}$) as well as longer truncations deleting the complete flexible C terminus (BsFtsZ$_{1-315}$), were still degraded similarly to full-length BsFtsZ$_{1-382}$. However, degradation was significantly impaired when we deleted the short N terminus of FtsZ (BsFtsZ$_{11-382}$, BsFtsZ$_{11-364}$, and BsFtsZ$_{11-315}$), identifying this structural feature as the preferred target site for ADEP-ClpP. Of note, all tested FtsZ protein variants were functional as shown in GTPase assays (see Fig. S2 in the supplemental material). We selected the synthetic derivative ADEP2 for all degradation assays in this study because, among a small series of ADEP congeners tested, it proved particularly effective at activating *B. subtilis* ClpP (BsClpP) for the degradation of BsFtsZ (see Fig. S3 in the supplemental material) and we had also used ADEP2 for degradation assays in our previous studies (14, 22). We further incubated FtsZ either alone or with ADEP (both in the absence of ClpP) for 60 min at 37°C, which did not affect FtsZ protein stability or functionality (see Fig. S4 in the supplemental material), ruling out off-target effects of ADEP on FtsZ or denaturing of FtsZ over the course of the *in vitro* assay.
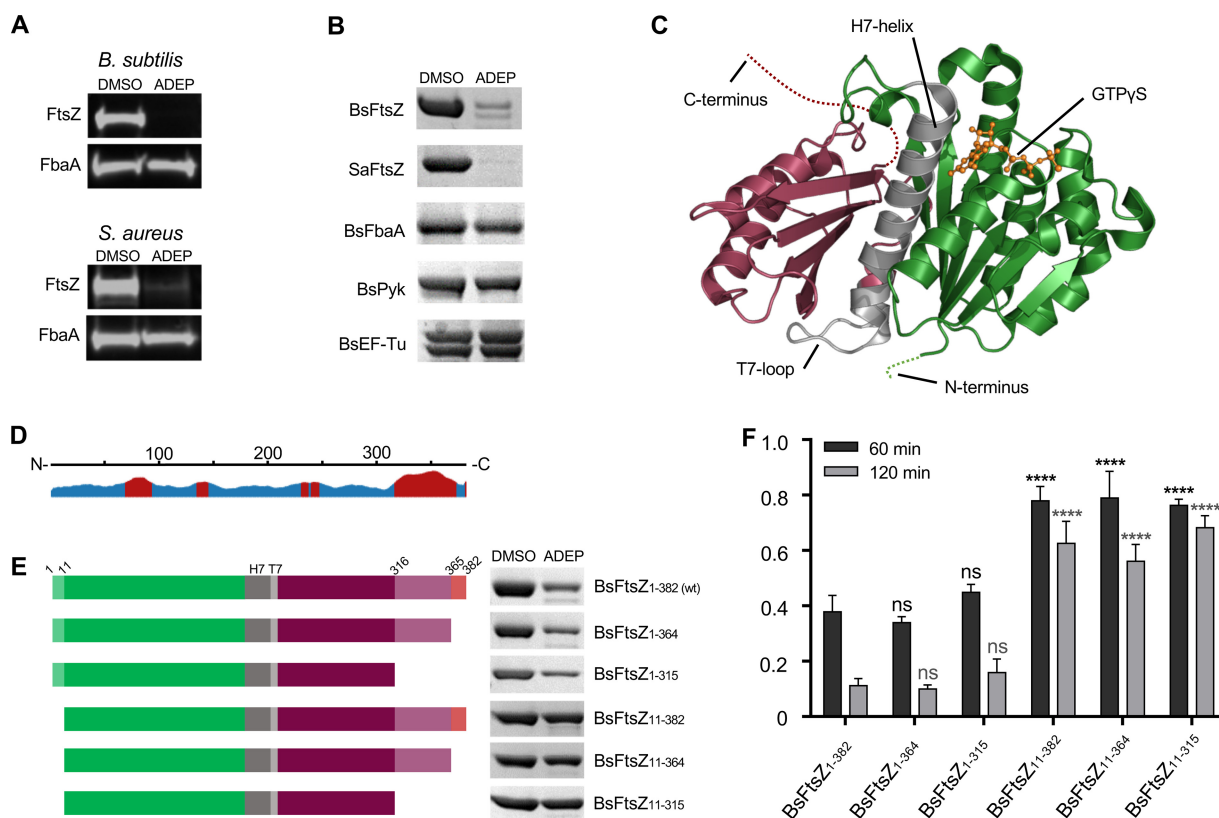
FIG 1 ADEP-activated ClpP preferentially targets the N terminus of FtsZ. (A) Immunoblotting of *B. subtilis* 168 and *S. aureus* NCTC8325 cells that were treated with ADEP concentrations close to the MIC (0.25 μg/ml ADEP2 for *B. subtilis* 168 and 1 μg/ml ADEP2 for *S. aureus* NCTC 8325), a concentration that leads to a pronounced filamentation phenotype of *B. subtilis* and swelling of *S. aureus*. Here, immunoblots show the rapid degradation of FtsZ compared with the untreated control (DMSO). In contrast, the abundance of FbaA was unaltered under the same conditions. Immunodetection of FtsZ and FbaA was performed using specific anti-FtsZ and anti-FbaA antibodies, respectively. Samples were taken after 120 min. DMSO was used as a control. (B) *In vitro* degradation assays using BsFtsZ and *S. aureus* FtsZ (SaFtsZ) as well as *B. subtilis* FbaA (BsFbaA), elongation factor Tu (BsEF-Tu), and pyruvate kinase (BsPyk) as purified protein substrates for ADEP-activated ClpP. In these assays, low concentrations of ADEP and ClpP were applied (1.5 μM ClpP; 1.5 μM ADEP). Samples were taken after 60 min. DMSO was used as a control. Of note, phosphorylation of BsEF-Tu often produces a doublet visible in SDS-PAGE, most probably resulting from partial phosphorylation of the multiply phosphorylated substrate (65). All experiments were performed at least in triplicate; representative images are depicted. (C) The crystal structure of *B. subtilis* FtsZ (BsFtsZ; Protein Data Bank entry 2RHO) bound to the nonhydrolyzable GTP-analog GTPγS shows two independently folding domains (24–26), the N-terminal domain harboring the nucleotide binding site (in green) as well as the C-terminal domain (in currant red). GTPγS is indicated in orange. Both domains are connected via the central H7 helix and the T7 loop (in gray). The short N terminus (amino acids 1 to 10) and the flexible C terminus (amino acids 316 to 382) are indicated by dotted lines. (D) Disorder prediction of BsFtsZ was computed with JRONN software (66) (Protein Data Bank entry 2RHO; https://www.rcsb.org). Predicted disordered regions (in red) and ordered regions (in blue) are indicated. (E) The left image panel provides a schematic representation of N- and C-terminal protein truncations of FtsZ used in degradation assays aligned to the disorder plot in D. The uppermost protein represents full-length FtsZ. The right image panel shows ADEP-ClpP degradation assays of full-length and truncated BsFtsZ proteins (aligned to the corresponding schematic on the left). In these assays, low concentrations of ADEP and ClpP were used (1.5 μM ClpP; 1.5 μM ADEP). Samples were taken after 60 min; DMSO was used as a control. (F) Densitometry of protein bands from SDS-PAGE was performed to compare FtsZ protein amounts in ADEP-treated samples with the corresponding DMSO control reactions after 60 min (black bars) and 120 min (gray bars). The respective DMSO control was set to 1.0 (100%). For each FtsZ variant, the data were collected from three different degradation assays and SDS-PAGE analyses using a standard curve. Protein amounts were calculated using a standard FtsZ concentration series that was applied on each SDS-PAGE. The plotted data depict the corresponding mean values, with standard deviations indicated by error bars. Compared with BsFtsZ$_{1-382}$, there was no significant (ns) difference regarding the remaining protein amount of the C-terminally truncated FtsZ mutant proteins BsFtsZ$_{1-364}$ and $_{Bs}$FtsZ$_{1-315}$ after 60 or 120 min of incubation with ADEP-ClpP. Contrariwise, the N-terminally truncated FtsZ proteins BsFtsZ$_{11-382}$, BsFtsZ$_{11-364}$, and BsFtsZ$_{11-315}$ were characterized by significantly less degradation of the FtsZ protein by ADEP-ClpP (****, $P < 0.0001$) than BsFtsZ$_{1-382}$. For all assays with substrates originating from *B. subtilis* or *S. aureus*, we used the corresponding BsClpP or *S. aureus* ClpP (SaClpP) proteins, respectively, with the according activity buffers (see Materials and Methods section). All results were confirmed by at least three independent experiments, and images of representative experiments are depicted.

Hydrophobicity of the FtsZ N terminus is important for degradation. The observation that ADEP-ClpP starts degradation at the N terminus of FtsZ was rather unexpected, raising the question of why the short N terminus should be preferred over the extended, flexible C terminus. To address this question, we analyzed the physicochemical properties of the N terminus of FtsZ *in silico*, and it emerged that it is overall hydrophobic in nature, in contrast to the C terminus of FtsZ (Fig. 2A). We thus
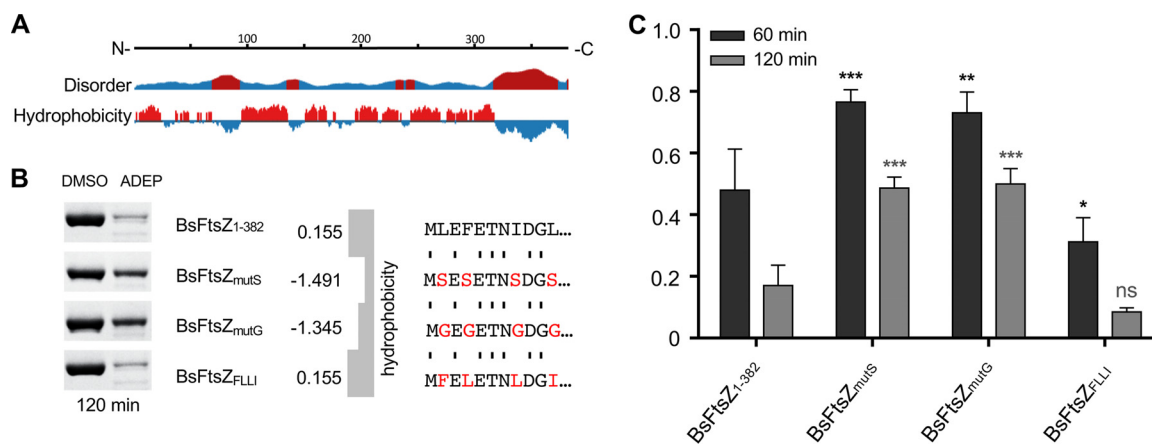
FIG 2 Hydrophobicity of the N terminus promotes FtsZ degradation. (A) Disorder prediction (top) and hydrophobicity prediction of FtsZ (bottom) were computed with JRONN software (66) (Protein Data Bank entry 2RHO; https://www.rcsb.org). Predicted disordered or hydrophobic regions are in red; ordered or hydrophilic regions are in blue. (B) ADEP-ClpP degradation assays of full-length, wild-type BsFtsZ$_{1-382}$ as well as of BsFtsZ$_{mutS}$ and BsFtsZ$_{mutG}$ mutant proteins (left image), which carry mutations that change the hydrophobicity of their N termini (right image). In addition, a BsFtsZ$_{FLLI}$ mutant protein was tested in which N-terminal hydrophobic amino acids were flipped, while overall hydrophobicity remained unchanged to wild-type FtsZ. The grand average of hydropathicity (GRAVY) of the mutated N termini was calculated according to the Kyte-Doolittle scale (67) using online software (https://web.expasy.org/protparam/). In these assays, low concentrations of ADEP and ClpP were used (1.5 μM ClpP; 1.5 μM ADEP). Samples were taken after a 120-min incubation; DMSO was used as a control. (C) Densitometry of protein bands from SDS-PAGE was performed to compare FtsZ protein amounts in ADEP-treated samples with the corresponding DMSO control reactions after 60 min (black bars) and 120 min (gray bars). The respective DMSO control was set to 1.0 (100%). For each FtsZ variant, the data were collected from three different degradation assays and SDS-PAGE analyses using a standard curve. The plotted data depict the corresponding mean values, with standard deviations indicated by error bars. Compared with BsFtsZ$_{1-382}$, BsFtsZ$_{mutS}$ and BsFtsZ$_{mutG}$ were significantly less degraded by ADEP-ClpP after incubation for 60 or 120 min. In contrast, FtsZ$_{FLLI}$ was similarly or slightly better degraded than BsFtsZ$_{1-382}$. *, $P < 0.05$; **, $P < 0.01$; ***, $P < 0.001$.

hypothesized that hydrophobicity may play a role in determining FtsZ as a target for ADEP-ClpP at low antibiotic concentrations and constructed functional mutant proteins with varied hydrophobicity of the N terminus. And indeed, the less hydrophobic mutant proteins BsFtsZ$_{mutG}$ and BsFtsZ$_{mutS}$, for which all hydrophobic amino acids of the N terminus were replaced by either glycine or serine, respectively, were clearly less prone to degradation by ADEP-ClpP (Fig. 2B and C), while retaining functionality in control GTPase assays (Fig. S2). When we exchanged the positions of the individual hydrophobic amino acids in BsFtsZ$_{FLLI}$ while keeping the overall hydrophobicity of this region unchanged, the mutant protein remained functional (Fig. S2) and was degraded similarly to full-length, wild-type BsFtsZ (Fig. 2B and C). This finding indicates that degradation of FtsZ does not depend on a certain amino acid sequence but that it is triggered by the hydrophobic nature of the N terminus.

The N terminus of FtsZ does not act as a universal degradation tag for ADEP-ClpP. We next wondered whether the hydrophobic N terminus of FtsZ may serve as a general degradation tag and would render proteins susceptible to ADEP-ClpP that otherwise resist degradation. To test this, we fused the N terminus of FtsZ (FtsZ$_{1-10}$) to enhanced green fluorescent protein (eGFP), a common model substrate for joint ClpP/Clp-ATPase complexes. However, neither attaching FtsZ$_{1-10}$ to the N terminus nor to the C terminus of eGFP resulted in its degradation by ADEP-ClpP (Fig. 3A). eGFP is known as a very stably folded protein that usually resists degradation by ClpP/Clp-ATPase complexes unless it is fused to a specific degron, which is recognized by the corresponding Clp-ATPase partner (28). Therefore, we also tested a fusion of FtsZ$_{1-10}$ to the Clp substrate Spx, but again, we did not observe degradation even after prolonged incubation with ADEP-ClpP (Fig. 3A), demonstrating that FtsZ$_{1-10}$ is not a degradation tag by itself that generally labels protein substrates for proteolysis by ADEP-ClpP. We then explored whether attaching the full-length FtsZ protein would trigger the degradation of eGFP by ADEP-ClpP. To this end, we constructed and purified a chimeric protein where eGFP is fused to the C terminus of full-length FtsZ, i.e., FtsZ-eGFP, which we then used in in vitro ADEP-ClpP degradation assays (Fig. 3B). As a control, we used
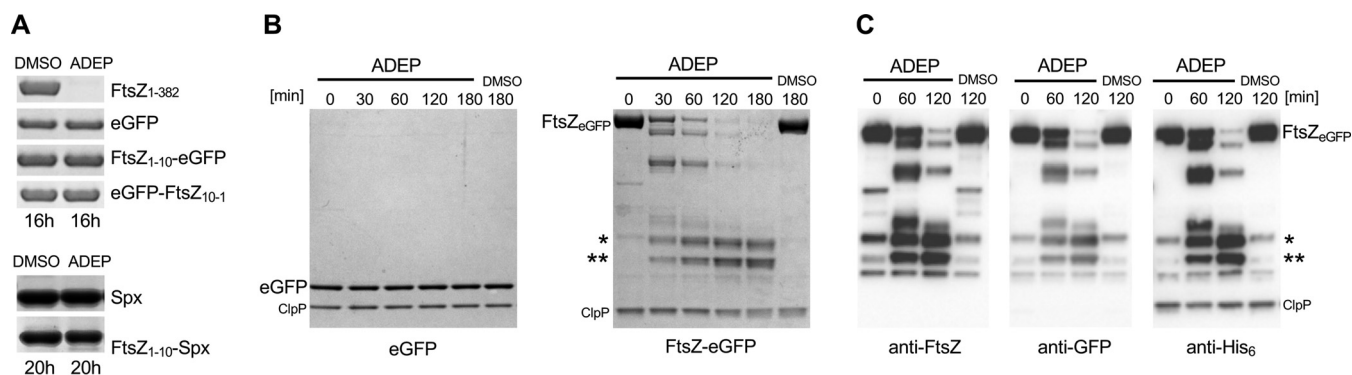
FIG 3 The N terminus of FtsZ is not sufficient to render proteins vulnerable to ADEP-ClpP. (A) *In vitro* ADEP-ClpP degradation assays of $FtsZ_{1-10}$ fused to either eGFP or Spx. For the fusion of $FtsZ_{1-10}$ to the C terminus of eGFP, the order of the N-terminal amino acids was inverted, which is indicated by $FtsZ_{10-1}$. (B) *In vitro* ADEP-ClpP degradation assays using eGFP alone as well as a fusion of eGFP to the C terminus of full-length FtsZ (FtsZ-eGFP). Here, eGFP alone resisted degradation, while FtsZ-eGFP was rapidly degraded, generating two accumulating degradation fragments over time (indicated by asterisks). (C) Immunoblotting of FtsZ-eGFP samples from ADEP-ClpP degradation assays using anti-FtsZ, anti-eGFP, and anti-His$_6$ antibodies. Of note, anti-FtsZ and anti-His$_6$ antibodies can be used to prove the integrity of the eGFP protein, as these antibodies recognize the C terminus of FtsZ and eGFP, respectively. The two accumulating degradation fragments of FtsZ-eGFP (indicated by asterisks) could be detected with all three antibodies, indicating an intact eGFP protein. In all assays, high concentrations of ClpP and ADEP2 were used (2.5 μM ClpP, 6.25 μM ADEP2). Samples were taken at indicated time points. DMSO was used as a control. All experiments were performed at least in triplicate; representative SDS-PAGE (A, B) or Western blot (C) images are depicted.

eGFP without FtsZ fusion, which resisted degradation by ADEP-ClpP. In our assay, FtsZ-eGFP was rapidly degraded, with two distinct degradation fragments accumulating over time. We further characterized these two fragments by immunoblotting using anti-His$_6$, anti-eGFP, and anti-FtsZ antibodies (Fig. 3C). Of note, the anti-FtsZ antibody used here recognizes the extreme C terminus of FtsZ, and the anti-His$_6$ antibody binds to the C-terminal His$_6$ tag of eGFP. Thus, anti-FtsZ and anti-His$_6$ antibodies can be used to confirm the integrity of the N and C terminus of eGFP, respectively, in this construct. Here, immunoblots showed that both accumulating fragments comprised full-length eGFP, since corresponding signals could be detected via all three antibodies. Corroborating the degradation of FtsZ from the N terminus, here ADEP-ClpP degraded the FtsZ part of the fusion protein FtsZ-eGFP, but it did not succeed in degrading eGFP even when fused to FtsZ. Obviously, FtsZ possesses additional inherent characteristics that only in combination with the hydrophobic N terminus permit degradation by ADEP-ClpP.

FtsZ cleavage extends into the folded N-terminal domain. FtsZ is efficiently degraded into smaller fragments, with a preferred degradation start at its N terminus (Fig. S1). However, one would expect that such degradation would require unfolding of the FtsZ protein in the absence of Clp-ATPases since the protein is presumably too large to access the proteolytic chamber in its folded form. One could speculate that the removal of the flexible N terminus (i.e., amino acids 1 to 10) might destabilize FtsZ such that it consequently unfolds on its own. However, our data demonstrate that the deletion of the flexible N-terminal portion leaves FtsZ folding intact. $BsFtsZ_{11-382}$ is functionally active in GTP hydrolysis (Fig. S2), and the truncated mutant is more stable than $BsFtsZ_{1-382}$ against degradation by ADEP-ClpP, making self-unfolding of the mutant protein highly unlikely. Furthermore, circular dichroism (CD) spectra of $BsFtsZ_{1-382}$, $BsFtsZ_{11-382}$ as well as untagged BsFtsZ in the absence or presence of the nonhydrolyzable GTP analogue guanosine-5′-O-(3-thiotriphosphate) (GTPγS) were superimposable. All spectra revealed the characteristic ellipticity of alpha-helical folds with two minima at 208 nm and 222 nm, indicating the presence of folded FtsZ proteins (without nucleotides as well as in the GTPγS-bound form) with similar average secondary structures under conditions that allow for the efficient degradation of full-length BsFtsZ (Fig. 4A). Therefore, we investigated whether ADEP-ClpP may be capable of destabilizing the fold of FtsZ during N-terminal attack to allow for further protein degradation.

To address this aspect of FtsZ proteolysis in more detail, we performed orienting analyses via label-free mass spectrometry (electrospray ionization-tandem mass spec-
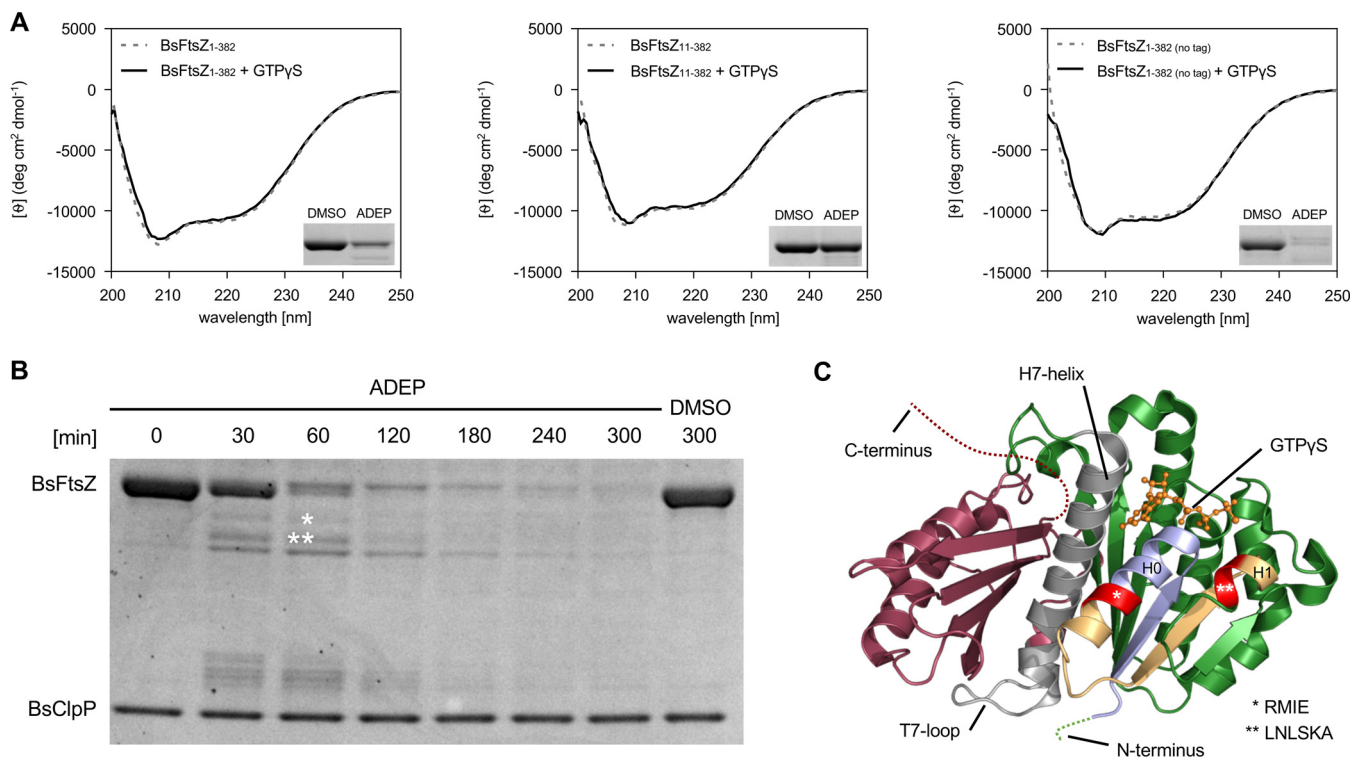
FIG 4 FtsZ folding and identification of early fragments of FtsZ degradation. (A) CD spectra of BsFtsZ$_{1-382}$ and BsFtsZ$_{11-382}$ (both C-terminally His$_6$ tagged) as well as BsFtsZ$_{1-382 \text{ (no tag)}}$ in the absence (gray dashed line) or presence of GTPγS (black line). All samples show the characteristic ellipticity spectra for an alpha-helical fold with two minima at 208 nm and 222 nm, indicating a folded state of the FtsZ protein under these conditions. As a control, *in vitro* degradation of the corresponding BsFtsZ proteins (without GTPγS) was performed using the CD buffer conditions (i.e., activity buffer CD) and low concentrations of ADEP and ClpP (1.5 µM ClpP, 1.5 µM ADEP, and 4 µM FtsZ). Samples were taken after 60 min; DMSO was used as a control. Representative images of duplicates are depicted. (B) Time course of BsFtsZ$_{1-382}$ degradation by ADEP-ClpP, indicating the generation of distinct degradation products. In these assays, low concentrations of ADEP and ClpP were used (1.5 µM ClpP, 1.5 µM ADEP, and 4 µM FtsZ). Samples were taken at indicated time points; DMSO was used as a control. Of note, when degradation reactions were allowed to continue, all depicted bands disappeared, indicating the capacity of ADEP-ClpP to fully digest FtsZ. The two largest of the emerging bands were excised (corresponding protein fragments are indicated by asterisks) and analyzed by Edman N-terminal protein sequencing. (C) Edman sequencing identified cleavage up to amino acid position 28 at the end of alpha-helix H0 (*RMIE) for the first fragment and up to position 49 of alpha helix H1 (**LNLSKA) for the second fragment (as indicated), which revealed that cleavage extends into the folded N-terminal domain of FtsZ. The crystal structure of GTPγS-bound BsFtsZ (Protein Data Bank entry 2RHO) highlights the first identified amino acid of both early fragments in red (the associated degradation product is indicated by asterisks) as well as the corresponding structural elements that are cleaved off by ADEP-ClpP (* in light blue, ** in light blue and yellow). GTPγS is indicated as the orange stick model.

trometry [ESI-MS]) of full-length and high-molecular-weight fragments of FtsZ, which indicated N-terminal truncations following degradation by ADEP-ClpP (see Fig. S5 in the supplemental material). To further corroborate this result, we next performed N-terminal protein sequencing by Edman degradation to identify early degradation fragments of wild-type FtsZ. Edman sequencing of the two largest degradation bands visible by SDS-PAGE (Fig. 4B) identified cleavage up to amino acid position 28 at the end of alpha-helix H0 (N-terminal amino acids determined by sequencing, RMIE) as well as up to position 49 of alpha helix H1 (N-terminal amino acids, LNLSKA). Thus, the data confirmed N-terminal degradation by ADEP-ClpP that extends into the folded region of the N-terminal domain of FtsZ (Fig. 4C).

Nucleotide binding prevents N-terminal degradation by stabilizing FtsZ. During the course of cell division, FtsZ assembles into protofilaments to form the "Z-ring" at the prospective division site, providing the scaffold for the assembly of the bacterial cytokinetic machinery. The formation of single-stranded protofilaments depends on GTP binding to FtsZ, which results in a dynamic head-to-tail association of individual FtsZ subunits (27, 29–33). The short hydrophobic N terminus of FtsZ can be assumed to be largely buried inside the binding interface between two subunits of an FtsZ protofilament (Fig. 5A). Therefore, we wondered whether the addition of GTP would have an impact on FtsZ degradation by rendering the N terminus less accessible to
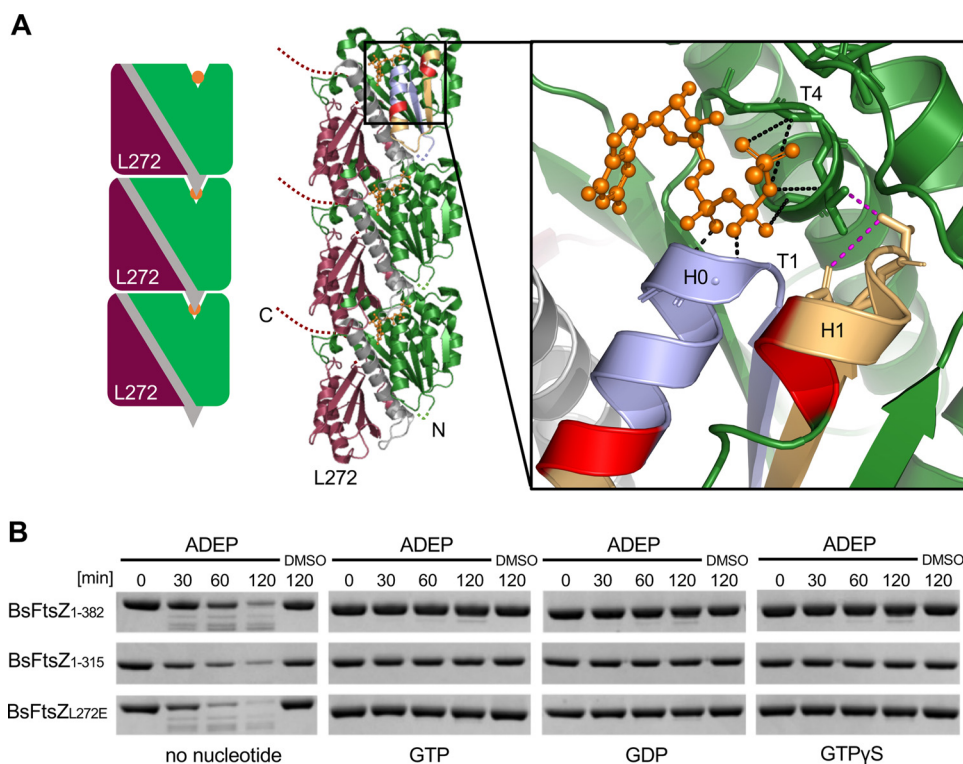
FIG 5 Nucleotide binding stabilizes FtsZ and inhibits degradation by ADEP-ClpP. (A) Head-to-tail association of individual FtsZ subunits result in single-stranded FtsZ protofilaments. The schematic shows the N-terminal domain (in green), the C-terminal domain (in currant red), and the central H7 helix with the T7 loop (in gray) as well as GTPγS (in orange). Also, the position of amino acid L272 inside the subunit interface is indicated. Note that in polymerized FtsZ, the short N terminus (N, green dotted line) is most probably largely buried in between two FtsZ monomers and may not be accessible to ADEP-ClpP. Zoom window shows established direct noncovalent contacts of GTPγS (in orange, Protein Data Bank entry 2RHO) with the T1 loop (Gly21-Gly22) and the T4 loop (Gly108-Gly110) (contacts in black) (37); the latter stabilizes helix H1 (contacts in magenta). The first amino acids of early FtsZ fragments, as identified by Edman sequencing (see Fig. 4), are indicated in red, cleaved off regions of the first and second degradation products in light blue and yellow, respectively. (B) ADEP-ClpP degradation assays of full-length BsFtsZ$_{1-382}$ as well as of BsFtsZ$_{1-315}$ and BsFtsZ$_{L272E}$ in the absence or presence of either GTP, GDP, or GTPγS. In these assays, low concentrations of ADEP and ClpP were used (1.5 μM ClpP; 1.5 μM ADEP). Samples were taken at indicated time points, DMSO was used as a control. All results were confirmed by at least three independent experiments, and images of representative experiments are depicted.

ADEP-ClpP. To test this, we preincubated FtsZ with GTP prior to ADEP-ClpP degradation and, indeed, preincubated FtsZ (BsFtsZ$_{1-382}$ and BsFtsZ$_{1-315}$) clearly resisted degradation, in contrast to the control which showed substantial proteolytic degradation in the absence of GTP (Fig. 5B). Also, preincubation with GDP, which mostly generates dimers or shorter, curved filaments of FtsZ (34–36), clearly inhibited the degradation of FtsZ. As a simple explanation for the observed protection from degradation, it might be speculated that the N terminus of FtsZ is hidden inside the protofilament and may, thus, be inaccessible to ADEP-ClpP (Fig. 5A, middle image).

Intriguingly, the N-terminal cuts detected by Edman sequencing require helices H0 and H1 to be pulled out of FtsZ, and these helices are located in the vicinity of the nucleotide binding site (Fig. 5A, right). Noteworthy, bound nucleotides establish direct noncovalent contacts with the T1 loop (Gly21-Gly22) and T4 loop (Gly108-Gly110) (37), the latter being part of the tubulin signature motif (GGGTGTG) which stabilizes helix H1 (Fig. 5A, right). As we hypothesized that FtsZ has to undergo unfolding during N-terminal degradation by ADEP-ClpP, we wondered if the sole binding of a guanosine nucleotide, regardless of protofilament formation, may already stabilize helices H0 and H1, thereby preventing FtsZ unfolding and subsequent degradation. To approach this hypothesis, we explored the impact of GTPγS that does not support protofilament formation. FtsZ polymerization cannot be induced by GTPγS that, however, still binds

to FtsZ (29, 38–41). And indeed, when we incubated FtsZ with GTPγS before the addition of ADEP-ClpP, thereby generating monomeric FtsZ bound to GTPγS, degradation was inhibited to the same extent as with GTP or GDP (Fig. 5B). To follow this route further, we employed a mutant FtsZ protein, BsFtsZ$_{L272E}$, which is capable of nucleotide binding but is impaired in GTP hydrolysis (Fig. S2). Accordingly, an *Escherichia coli* FtsZ$_{L272E}$ mutant had previously been described to exist only in the monomeric, nonpolymerized form, as L272 is located inside the biologically relevant intersubunit interface (42). In accordance with the results obtained for monomeric wild-type FtsZ bound to GTPγS, BsFtsZ$_{L272E}$ resisted degradation by ADEP-ClpP when preincubated with either GTP, GDP, or GTPγS (Fig. 5B). Although FtsZ (without the addition of nucleotides) appears to be in a folded state with similar average secondary structures under conditions allowing FtsZ degradation *in vitro* (Fig. 4A), nucleotide binding alone is sufficient, without the need of protofilament formation, to further stabilize the overall fold of the N-terminal domain of FtsZ and to prevent degradation of FtsZ from the N terminus.

The C terminus of FtsZ is increasingly degraded at higher concentrations of ADEP-ClpP. As detailed above, degradation of FtsZ by ADEP-ClpP preferentially starts from the N terminus, and low ADEP/ClpP concentrations (1.5 μM ClpP; 1.5 μM ADEP) were sufficient for efficient degradation of the entire protein into small fragments. FtsZ mutants lacking the short flexible N terminus remained largely intact when exposed to ADEP at these low concentrations. Nonetheless, in degradation assays using N-terminally truncated BsFtsZ$_{11-382}$ (Fig. 1E) or nucleotide-bound FtsZ$_{1-382}$ (Fig. 5B), a single faint band appeared slightly below the band of the full-length protein after prolonged incubation with ADEP-ClpP. The slow appearance of this band, its large size, and the fact that it was not readily degraded further oppose an origin from a fraction of residual unfolded or nucleotide-free FtsZ. Rather, these findings pointed toward a second target site within FtsZ to be degraded with considerably lower efficiency. We thus increased the concentration of ADEP and ClpP in our *in vitro* assay system (1.5 μM ClpP, 3.75 μM ADEP2 as well as 2.5 μM ClpP, 6.25 μM ADEP2; both correspond to 2.5 molar surplus of ADEP) and tested if we could also trigger degradation of nucleotide-bound FtsZ. And indeed, nucleotide-bound FtsZ was increasingly degraded at higher concentrations of ADEP/ClpP indicated by the appearance of more pronounced degradation fragments (Fig. 6A). Of note, degradation was also observed when using GTP, GDP, or GTPγS with FtsZ$_{L272E}$. Since the N terminus is stabilized in nucleotide-bound FtsZ, we hypothesized that the C terminus might serve as a secondary target site at higher concentrations of ADEP/ClpP. To further explore this, we tested the degradation of nucleotide-bound BsFtsZ$_{1-315}$ which lacks the flexible C terminus. In fact, the addition of nucleotides prevented the truncation of BsFtsZ$_{1-315}$, and no degradation bands appeared even at higher concentrations of ADEP/ClpP (Fig. 6A; see Fig. S6A in the supplemental material). C-terminal attack was also confirmed *in vitro* by immunoblotting using a His$_6$ tag fused to the C terminus of FtsZ (Fig. S6B). Likewise in whole cells, ADEP-ClpP truncated the C terminus of FtsZ when the N terminus was blocked with GFP, generating a stable degradation product only slightly smaller than FtsZ itself (see Fig. S7A in the supplemental material). In contrast, when GFP blocked the C terminus of FtsZ, FtsZ appeared fully degraded by ADEP-ClpP. Interestingly, we did not detect an accumulation of GFP fragments in the whole-cell situation that should have derived from an FtsZ-only degradation of the FtsZ-GFP fusion protein (Fig. S7B), as seen in our *in vitro* assays (Fig. 3C). Thus, we cannot exclude that FtsZ-GFP or fragments thereof may be fully degraded by ADEP-ClpP alone or with the help of other proteases in the bacterial cell, including degradation of GFP under these conditions.

We then gradually increased the ADEP concentration in our *in vitro* degradation assay, while keeping the ClpP concentration constant at 1.5 μM, and analyzed the degradation of the proteins BsFtsZ$_{1-382}$, BsFtsZ$_{11-382}$, and BsFtsZ$_{1-315}$ (Fig. 6B). Here, the degradation of BsFtsZ$_{1-382}$ was clearly increased at more than 2-fold the molar con-
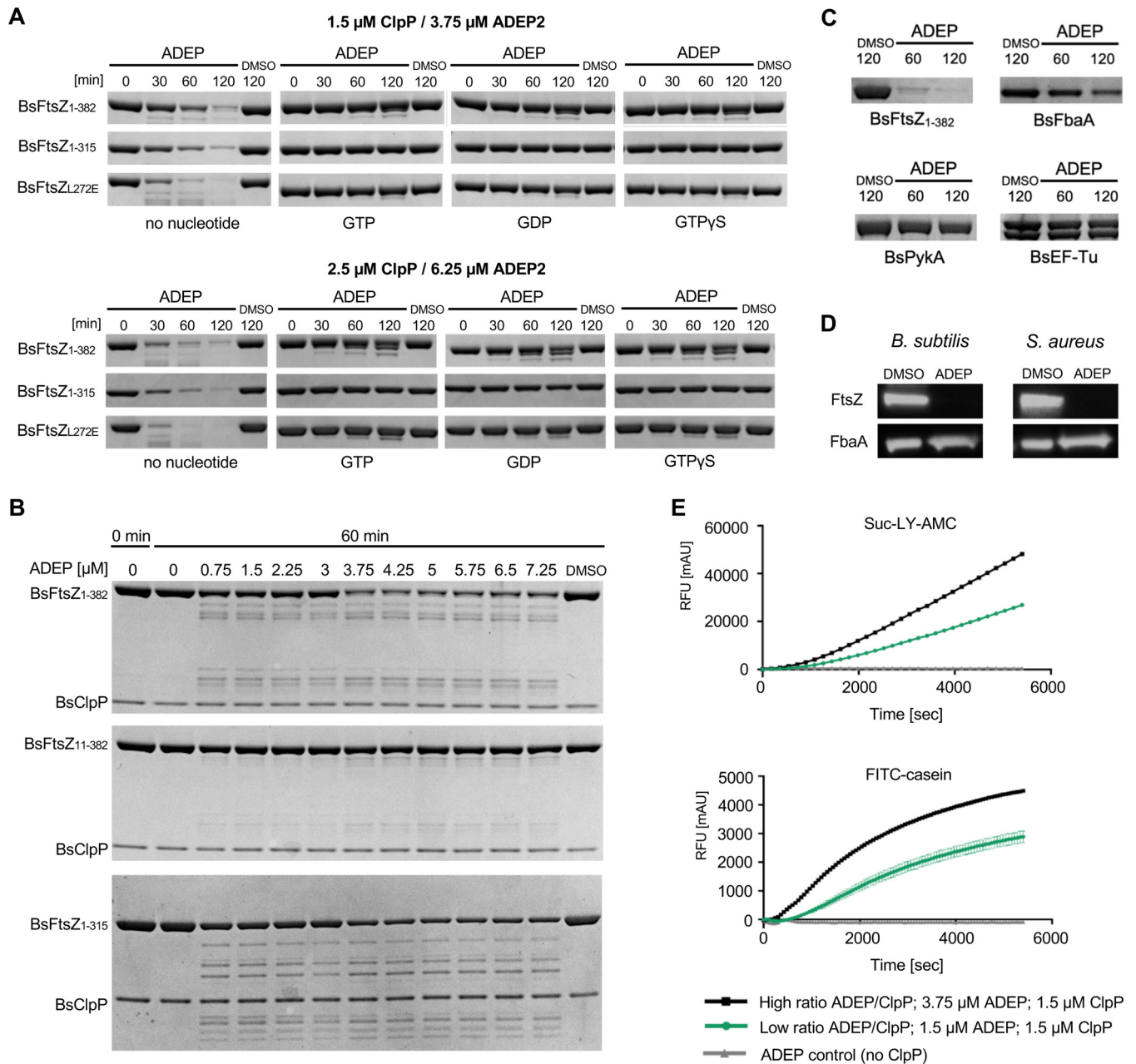
FIG 6 High concentrations of ADEP over ClpP lead to the degradation of the C terminus of FtsZ. (A) ADEP-ClpP degradation assays of BsFtsZ$_{1-382}$, BsFtsZ$_{1-315}$, or BsFtsZ$_{L272E}$ in the absence or presence of guanosine nucleotides using increased concentrations of ADEP over ClpP (top, 1.5 μM ClpP and 3.75 μM ADEP2; bottom, 2.5 μM ClpP and 6.25 μM ADEP2). DMSO was used as a control. Results were confirmed by at least three independent experiments, and images of representative experiments are depicted. (B) Degradation of BsFtsZ$_{1-382}$, BsFtsZ$_{11-382}$, or BsFtsZ$_{1-315}$ in the presence of 1.5 μM ClpP and increasing concentrations of ADEP2 (0 to 7.25 μM). Samples were taken after 60 min. DMSO was used as a control. Results were confirmed by at least three independent experiments, and images of representative experiments are depicted. (C) ADEP-ClpP degradation assays using BsFtsZ$_{1-382}$, BsFbaA, BsEF-Tu, or BsPyk as substrates for ADEP-activated ClpP at a high concentration of ADEP over ClpP (2.5 μM ClpP; 6.25 μM ADEP). Samples were taken at indicated time points. DMSO was used as a control. Of note, phosphorylation of BsEF-Tu produces a doublet band resulting from partial phosphorylation of a multiply phosphorylated substrate (65). All experiments were performed at least in triplicate; representative images are depicted. (D) Immunoblotting of *B. subtilis* 168 or *S. aureus* NCTC8325 cells that were treated with high ADEP concentrations (3 μg/ml ADEP for *B. subtilis* 168 and 8 μg/ml ADEP2 for *S. aureus* NCTC 8325, i.e., 10× MIC), leading to growth arrest due to ceased biomass production. Here, immunoblots indicated the rapid degradation of FtsZ compared with the untreated control (DMSO). In contrast and despite the increased ADEP concentration, the abundance of FbaA remained unaltered in both species over time. Immunodetection of FtsZ or FbaA was performed using specific anti-FtsZ or anti-FbaA antibodies, respectively. Samples were taken after 120 min. (E) Effects of low and high concentrations of ADEP on peptidase activity using the fluorogenic peptide substrate Suc-LY-AMC (top) or on protease activity using the fluorogenic protein substrate FITC-casein (bottom), respectively. Quenched 7-amino-4-methylcoumarin (AMC) fluorescence is released upon peptide hydrolysis (top). Quenched FITC fluorescence is released upon proteolysis (bottom). Reaction rates per 1.5 μM BsClpP in relative fluorescence units (RFUs) during the linear phase of substrate degradation. DMSO was used in control reactions and was subtracted from corresponding ADEP values. The reaction in the absence of ClpP was used as an additional control. Assays were confirmed in at least three independent experiments. Error bars for Suc-LY-AMC and FITC-casein assays indicate standard deviations.

centration of ADEP (starting at 3.75 μM ADEP2) over the ClpP monomer concentration. In accordance with our data described above, the degradation of BsFtsZ$_{11-382}$ was mostly prevented at lower ADEP/ClpP ratios but was triggered at higher ADEP concentrations, indicated by the appearance of pronounced degradation fragments, as a result of increased C-terminal degradation of FtsZ under these conditions. Also, N-terminal degradation of FtsZ was reproducibly accelerated at higher ADEP/ClpP ratios since BsFtsZ$_{1-315}$ was also increasingly degraded. To further test an ADEP/ClpP concentration-dependent degradation of other proteins, we attempted the degradation of BsEF-Tu, BsPyk, and BsFbaA using high ADEP/ClpP concentrations in our *in vitro* assays (Fig. 6C). While BsEF-Tu and BsPyk still resisted degradation under these conditions, the amount of BsFbaA slightly decreased over time, suggesting its degradation by ADEP-ClpP. However, when we employed immunoblotting to test the abundance of FbaA in *B. subtilis* and *S. aureus* cells that had been treated with high ADEP concentrations ($>$10$\times$ MIC), the protein concentration of BsFbaA still remained unaltered under these conditions, in contrast to BsFtsZ (Fig. 6D). Thus, it cannot be excluded that either a portion of the FbaA protein batch used in our *in vitro* assay may not have been properly folded, which may lead to its degradation, or that FbaA is sufficiently replenished by protein expression or its fold may be stabilized in the bacterial cytoplasm, impeding its degradation.

Our data consistently indicate that the flexible C terminus of FtsZ is targeted at higher concentrations of ADEP/ClpP in addition to the N terminus. To explore the molecular rationale for this observation, we tested the peptidase and protease activity of ADEP-ClpP under the same assay conditions (low versus high concentration of ADEP/ClpP). By studying the degradation of the peptide substrate Suc-Leu-Tyr-7-amino-4-methylcoumarin (Suc-LY-AMC) (Fig. 6E, top graph) or the loosely folded protein model substrate fluorescein isothiocyanate-casein (FITC-casein) (Fig. 6E, bottom graph), both the peptidolytic and proteolytic degradation rate of ADEP-activated ClpP were notably increased when the concentration of ADEP was raised. However, it is a matter not only of degradation velocity but also of selection capability, as a further target structure (the C-terminal end in addition to the N terminus of FtsZ) is addressed under these conditions. Hence, our data indicate that the destructive quality of ClpP increases with rising concentrations of ADEP, i.e., the spectrum of efficiently degraded substrates by ADEP-ClpP is widened. In the treated cell, this probably reflects the degradation of additional target structures, of which the C terminus of FtsZ is only but one example. Our results on FtsZ thus show that the fate of a protein, when targeted by ADEP-ClpP, depends not only on the capabilities of the deregulated protease but also on protein-intrinsic fragile or stabilizing substructures as well as physiochemical properties.

DISCUSSION

ADEP antibiotics have a dual mechanism of antibacterial action that is based on the multilayered deregulation of bacterial protease Clp; by binding to ClpP, ADEP inhibits all Clp functions in the bacterial cell (13, 14), and at the same time, it activates ClpP for the proteolysis of nonnative substrates in the absence of regulatory Clp-ATPases (1, 13, 17, 22). Depending on the bacterial species, ADEP uses either one or the other mechanisms for bacterial killing (1, 14). With regard to ClpP activation for the Clp-ATPase-independent degradation of nonnative substrates, we previously observed the following two concentration-dependent phenotypes in *B. subtilis*: (i) at ADEP concentrations several times the MIC, biomass increase ceased early (22, 23) and treated cells remained small, suggesting a depletion of essential proteins in various processes of the bacterial metabolism; and (ii) in contrast, at ADEP concentrations close to the MIC, treated cells were characterized by a phenotype of extensive filamentation, clearly marking an inhibition of cell division as the major antibiotic effect at these antibiotic concentrations. This filamentation phenotype is due to the untimely degradation of FtsZ (22), the pacemaker protein of cell division in most bacteria (30, 31). In fact, our new data show that the FtsZ protein seems especially prone to degradation compared

with other proteins, such as FbaA, EF-Tu, or Pyk, although FtsZ is most probably not the only cellular protein substrate of ADEP-ClpP, and nascent polypeptides at the ribosome are ADEP-ClpP targets as well (1, 13). In this context, it is further noteworthy that ADEP-activated BsClpP is even capable of degrading FtsZ from different species, including *Mycobacterium tuberculosis* (14). However, the reason for such a preferential degradation of FtsZ at low inhibitory ADEP concentrations has remained elusive so far.

In the current report, we now provide insight into the mechanism of FtsZ degradation by ADEP-ClpP which emerged to occur stepwise at different structural sites of FtsZ, depending on the applied concentration of ADEP and ClpP. At low concentrations of ADEP/ClpP, our results show that degradation by ADEP-ClpP preferably starts at the short N terminus of FtsZ. This finding was rather unexpected because the N-terminal region of FtsZ, which extends beyond the globular protein structure, is too short to reach the secluded catalytic sites of the ADEP-activated ClpP tetradecamer without the need of unfolding FtsZ. Assuming that the accessible part of the FtsZ N terminus is an extended peptide chain without secondary structure, its calculated length according to the Pauling model would be 36 Å (10 amino acids, 3.6 Å each for an extended peptide chain) (43, 44). However, a polypeptide chain would need to cover a distance of at least 40 Å from the entrance pore of the ADEP-ClpP tetradecamer (Glu53) to the active site serine (S97) of the catalytic triads (19). In contrast, the extended, flexible C terminus of FtsZ with a theoretical length of more than 200 Å would be long enough by far to easily diffuse through the opened pores of a ClpP tetradecamer to reach the catalytic triad and be degraded. Although the entrance pore diameter changes from ~1.8 nm in apo-BsClpP to ~2.7 nm in ADEP-bound BsClpP (19), it is still not wide enough to allow for entry of the N-terminal domain of FtsZ in its folded state (diameter, ~4 nm) into the degradation chamber, which implies that the N terminus of FtsZ needs to unfold during attack by ADEP-ClpP. A mechanism of protein unfolding is further supported by our observation that nucleotide binding to FtsZ prevents degradation at the N terminus, most probably by stabilizing the overall fold of the N-terminal domain of FtsZ. To our best knowledge, ClpP has not been described before to lead to protein unfolding in the absence of an associated Clp-ATPase, which usually unfolds Clp target proteins in an energy-dependent manner and upon recognition of a specific degron, such as SsrA (28). In *Escherichia coli*, for example, ClpX identifies FtsZ as a Clp target via two recognition signals located near the C terminus of FtsZ (45, 46). In this context, we have previously attempted the degradation of native Clp protease substrates using ADEP-ClpP, including MecA, McsB, and ComK from *B. subtilis* or DnaK, TigA, or GroEL from *E. coli*, as well as SsrA-tagged GFP, which all resisted degradation by ADEP-ClpP in our *in vitro* assays (22). On the other hand, FtsZ appears not to be degraded by ClpXP in *B. subtilis* (47, 48), indicating that the recognition of substrates by the Clp protease fundamentally differs from the substrate preference of ADEP-ClpP.

FtsZ has not principally been regarded as intrinsically unstable or loosely folded (25, 26, 30, 31). However, as FtsZ is a preferential target of ADEP-ClpP, which implies special inherent characteristics of the FtsZ protein, it may well be that the stability of the N-terminal domain of FtsZ (when devoid of nucleotides) is lower than that of other cytoplasmic proteins (49). Several studies reported on the presence of an unfolding intermediate of FtsZ and suggested that intradomain stabilization is important for overall protein stability (49–52). Since the N- and C-terminal domains of FtsZ represent independent folding domains (24), one could envision that partial unfolding of FtsZ, where the N-terminal half becomes unfolded and unbound from the C-terminal half of the polymerization domain, would allow for the exposure of a region smaller than the 2.7-nm diameter of the ADEP-bound BsClpP pore. Very recently, it has been reported that under certain *in vitro* conditions *S. aureus* FtsZ would occur in an unfolded state and requires nucleotide binding for proper folding (53). Although FtsZ was not intrinsically unfolded in our *in vitro* conditions, as shown by our CD data that indicate a normal FtsZ secondary structure fold with no difference in the absence or presence of nucleotides, this finding is very intriguing regarding the general stability of the FtsZ protein. Our data on the preferred degradation of FtsZ by ADEP-ClpP further support

the notion of a rather fragile fold of the FtsZ protein (under *in vitro* conditions as well as in the living cell) compared with other tested cellular proteins, including natural Clp substrates or eGFP. We therefore suggest that upon direct binding, ADEP-ClpP exploits such intrinsic conformational flexibility of the folded FtsZ protein (or at least of its N-terminal domain), leading to protein unfolding and subsequent digestion. Such intrinsic flexibility of a protein's fold may be a prerequisite for protein substrates of ADEP-ClpP, a degradative machine not supported by protein unfolding via energy-dependent Clp-ATPases.

Our data show that hydrophobic interactions play a pivotal role in the degradation of the N-terminal region of FtsZ by ADEP-ClpP, which may provide an explanation for the observed phenomenon. Hydrophobic residues also cluster around the rim of the ClpP entrance pore (54), and the inner surface of the degradation chamber is largely hydrophobic as well (55). Since the hydrophobic effect is considered the major driving force for the folding of proteins, strong enough to trigger supramolecular assemblies (56), establishing new hydrophobic contacts between FtsZ and ADEP-ClpP might weaken intrinsic contacts within FtsZ itself and lead to its unfolding. We therefore propose that the N terminus of FtsZ establishes hydrophobic contacts with the entrance pore of ClpP and beyond within the degradation chamber and that the sum of such interactions might be sufficient to allow the N terminus of FtsZ to partially unfold and stretch further into the degradation chamber of ClpP, leading to a destabilization of the N-terminal protein fold of nucleotide-free FtsZ (Fig. 7).

At higher concentrations of ADEP/ClpP, our data show that the spectrum of effectively degraded substrates by ADEP-ClpP is broadened, as we observed the additional degradation of the C terminus of FtsZ when using excess ADEP over ClpP, a substructure which mostly resisted degradation at lower concentrations of ADEP/ClpP. The molecular reason for such a broadening of the ADEP-ClpP substrate spectrum remains currently unclear and deserves further study. However, although equimolar concentrations of ADEP and ClpP were used for the condition of "low concentration of ADEP/ClpP" in our assays, it is feasible that the ClpP tetradecamer may not be saturated with ADEP molecules under these conditions. In all available crystal structures of ADEP-ClpP, all hydrophobic pockets of ClpP were fully occupied (2, 19, 20, 57, 58), the entrance pores were widened to the extent described above, and all catalytic sites were captured in the active conformation. However, crystal structures present a static endpoint generated at very high protein and compound concentrations. In a dynamic constellation, lower versus higher concentrations of ADEP may well influence ClpP occupancy, pore dynamics, and active site activity, which may lead to a preference for certain targets, such as the N terminus of FtsZ, over others. In our study, we observed a two-step activation mechanism of ClpP regarding FtsZ degradation, where degradation efficiency visibly increased at more than 2-fold the molar excess of ADEP over ClpP (Fig. 6B), that may therefore reflect unsaturated and saturated states of the ClpP tetradecamer with respect to ADEP binding.

FtsZ assembles into protofilaments to eventually form the Z-ring at midcell and initiate cell division. FtsZ protofilament formation is characterized by a continuous binding and consumption of GTP, which is then released as GDP from FtsZ to allow the binding of a new GTP molecule. This constant exchange of nucleotides is accompanied by the dynamic exchange of FtsZ subunits between the Z-ring and the cytoplasmic pool (27, 29–33). Importantly, a certain critical concentration of FtsZ is required for protofilament formation (29, 59). Our data show that nucleotide-bound FtsZ resists proteolytic attack at lower ADEP concentrations. In the context of bacterial cell division, it may therefore be hypothesized that ADEP-ClpP will predominantly deplete the cytoplasmic pool of apo-FtsZ when low inhibitory ADEP concentrations are used. This may consequently lead to a reduction of the cytoplasmic FtsZ level below the critical concentration required for filamentation, which will inevitably result in an inhibition of cell division and eventually cell death. At higher ADEP concentrations, we showed that nucleotide binding does not prevent FtsZ degradation by ADEP-ClpP since the C terminus becomes an additional target independent of the presence of bound
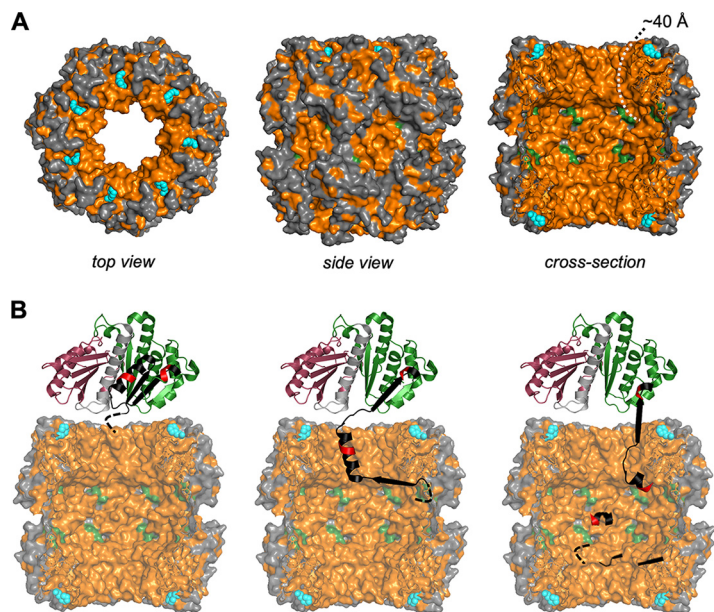
FIG 7 Proposed model for the N-terminal degradation of FtsZ by ADEP-ClpP. (A) Crystal structure of a *B. subtilis* ClpP tetradecamer (BsClpP; Protein Data Bank entry 3KTK; in gray with overall hydrophobic regions in orange) with ADEP2 bound to the hydrophobic pockets (cyan). Catalytic triads are highlighted in green. The cross-section of a BsClpP tetradecamer (right) models the inside of the proteolytic chamber, illustrating the overall hydrophobic nature of the ClpP entrance pore (54) and the inner surface of the degradation chamber (55). Noteworthy, in the available BsClpP crystal structure, the outermost N-terminal amino acids lining the entrance pore are not visible due to inherent flexibility. Thus, the actual situation regarding the hydrophobic surface interacting with an unfolded FtsZ N terminus or any unfolded protein will slightly deviate from what is shown here. To reach the catalytic triads within the proteolytic chamber, a peptide chain has to span a length of approximately 40 Å. (B) Hydrophobic interactions appear to be important for the attack of ADEP-ClpP on the N-terminal region of FtsZ since the hydrophobicity of the FtsZ N terminus supports its degradation. We propose that the hydrophobic N terminus of FtsZ (black dashed line) engages with ClpP via manifold hydrophobic interactions that occur within the entrance pore of ClpP and beyond within the degradation chamber. A sum of interactions that is, in total, stronger than the binding forces within the FtsZ N-terminal domain itself, supported by a nonstatic nature of the ClpP pore surface, might trigger an unfolding process that allows the N terminus of FtsZ to extend further and yet further into the catalytic chamber. Although ClpP alone might not "pull" by force, as the Clp-ATPases can do during their ATP-fueled power stroke, it might still be perfectly capable of "holding tight" long enough to destabilize the secondary structure within the potentially rather flexible N-terminal domain of nucleotide-free FtsZ (in black and green). Nucleotide binding, however, prevents FtsZ unfolding by stabilizing the N-terminal domain and thus inhibits degradation of the N terminus.

nucleotides. Here, the grappling hook peptide (GHP) (60) located at the extreme C terminus of FtsZ is degraded, which represents the interaction interface of FtsZ with other divisome proteins. Hence, C-terminal degradation will further contribute to a depletion of intact FtsZ available for Z-ring formation, thus accelerating the detrimental effects on cell division.

In conclusion, our data identify the hydrophobic N terminus of FtsZ as a preferred target at low levels of ADEP/ClpP, although it cannot be excluded that further proteins are also degraded at filamentation concentrations but show a less prominent phenotype. A stepwise degradation of distinct target structures by ADEP-ClpP as indicated here provides a rationale for the series of events that lead to the strikingly different phenotypes at low versus high ADEP concentrations (prolonged filamentation versus rapid cessation of biomass production, respectively) (23). This suicide-like mechanism of protease activation with its broad destructive capacity is distinct from all clinically applied antibiotics and makes ADEPs a promising starting point for the development of novel strategies for antibacterial attack.

MATERIALS AND METHODS

Bacterial strains and growth conditions. Bacterial strains and plasmids used in this study are listed in Table S1 in the supplemental material. Bacteria were grown in lysogeny broth (LB) at 37°C, which was

supplemented with appropriate antibiotics or inducing compounds when required. ADEP2 was added to early-exponential-phase *B. subtilis* or *S. aureus* cultures unless otherwise stated. For low (2× to 3× MIC) or high (>10× MIC) ADEP2 concentrations, 0.25 μg/ml or 3 μg/ml ADEP2 was used for *B. subtilis* and 1 μg/ml or 8 μg/ml ADEP2 for *S. aureus*, respectively. Of note, the ADEP per ClpP (ADEP/ClpP) molar ratios occurring in bacterial cells when exposed to the low and high ADEP concentrations in our whole-cell assays may, of course, differ from the ADEP/ClpP ratios adjusted in our *in vitro* assays. The actual ADEP concentrations in the two distinct settings were chosen for the following reasons: *in vitro*, the low and high concentrations were selected to clearly differentiate between the N-terminally focused degradation and the combined N-/C-terminal attack. In the whole-cell context, the low concentration leads to a strong filamentation phenotype in *B. subtilis* (respective swelling in *S. aureus*) and thus a phenotype dominated by FtsZ degradation, whereas under the high concentration, biomass increase and metabolism in general are severely inhibited, demonstrating degradation of a wider range of substrates. MICs were determine according to the guidelines of the Clinical and Laboratory Standards Institute (CLSI) except for using LB.

Cloning experiments. Primers that were used for cloning experiments in this study are listed in Table S2 in the supplemental material. Polymerase, T4 ligase, and antarctic phosphatase as well as restriction enzymes that were used for cloning experiments were obtained from New England BioLabs (NEB). Genes were amplified from genomic DNA of *B. subtilis* 168 (*clpP*, *ftsZ*, *fbaA*, *pyk*, and *tufA*) or *S. aureus* NCTC 8325 (*clpP* and *ftsZ*) (Table S1 and S2). The sequence of *egfp* was amplified using the plasmid pDest007-eGFP-(Ec)-ssrA (17). For ligation, a vector:insert ratio of 1:5 was employed using 70 ng of the double digested and dephosphorylated vector. PCR products were purified and digested with respective enzymes and ligated into expression vector pET22b or pET11a as indicated. For attaching purification tags or the N terminus of FtsZ, corresponding DNA fragments were amplified from template plasmids (indicated in Table S2) using either 5′-phosphorylated oligonucleotides or oligonucleotides with the same restriction site. The plasmids pET11a-bsPyk and pETftsZbs-egfp$_{H6}$ were cloned using the Gibson assembly master mix (NEB). For plasmid pETftsZbs-egfp$_{H6}$, a linker comprising 24 bp was inserted between the sequence of *ftsZ* and *egfp* to support correct protein folding and to allow sufficient flexibility of the protein fusion (the linker region is highlighted in gray in Table S2). Plasmid pETftsZbs$_{L272E}$ was generated using the QuikChange II site-directed mutagenesis kit (Agilent Technologies). Primers were constructed as described according to the manufacturer's manual.

Protein purification of ClpP and FtsZ. Native FtsZ of *B. subtilis* 168 was expressed in *E. coli* strain W3110 (pBS58) (pCXZ), as described earlier (22, 61). His$_6$-tagged FtsZ and ClpP proteins (originating from *B. subtilis* 168 or *S. aureus* NCTC8325) were expressed in *E. coli* BL21(DE3) harboring the respective expression plasmid (Table S1) and were purified as previously described (62). The quality and quantity of purified proteins were verified by SDS-PAGE, Bradford assay (using bovine serum albumin as the control), and spectrophotometry (Nanodrop Technologies). All tested FtsZ mutant proteins in this study were catalytically active, as shown by GTPase activity assays (GTPase-Glo assay; Promega) (Fig. S2), and the use of purification tags had no effect on degradation preference (see Fig. S8 in the supplemental material).

GTPase activity assays. The functionality of wild-type and mutant FtsZ proteins was analyzed using the GTPase-Glo assay (Promega) according to the manufacturer's instructions (Fig. S2). The assay measures the amount of residual GTP after a GTPase reaction by converting remaining GTP into ATP that is then detected using a luciferin/luciferase reaction. Different FtsZ concentrations were incubated in a white 384-well microtiter plate (Brand) for 1 h at 25°C in the presence of 5 μM GTP and 1 mM DTT in GTPase/GAP buffer (volume, 10 μl). An equal volume of GTPase/Glo buffer was then added, and the reaction mixture was incubated for 30 min at 25°C while shaking. For the luciferin/luciferase reaction, 20 μl of the detection reagent was added to each well, and the luminescence was measured in a microplate reader (Tecan Infinite M200) after 10 min.

Circular dichroism. FtsZ proteins were used at a concentration of 3.5 μM in activity buffer CD (50 mM Tris/HCl [pH 8], 25 mM MgCl$_2$, and 100 mM KCl) in the absence or presence of 40 μM GTPγS. To allow nucleotide binding by FtsZ, samples were preincubated for 10 min at room temperature before the start of the measurement. CD spectra were recorded from 200 to 250 nm (1-nm bandwidth, 20-nm min^{-1} scanning speed) with a Jasco J-720 spectropolarimeter using a 1-mm cuvette. The spectra were recorded 10 times for each protein sample, averaged, and corrected for the buffer system (with or without GTPγS, respectively). Spectra were only shown in the range of 200 nm to 250 nm since the activity buffer CD contains ions that strongly absorb at lower wavelengths.

***In vitro* nucleotide binding and degradation assays.** For *in vitro* guanosine nucleotide binding, FtsZ proteins (4 μM) were incubated in activity buffer BS (50 mM Tris/HCl [pH 8], 25 mM MgCl$_2$, and 100 mM KCl, 2 mM DTT) for *B. subtilis* proteins or activity buffer SA (20 mM HEPES [pH 7], 100 mM NaCl) for *S. aureus* proteins. Desired guanosine nucleotides were added to the reaction mixture to a final concentration of 1 mM according to a method described previously (63). For *in vitro* degradation, target proteins (4 μM BsPyk, BsEF-Tu, BsFbaA, eGFP, BsFtsZ-eGFP, and nucleotide-free or nucleotide-bound FtsZ) were incubated at 37°C in activity buffer BS (for *B. subtilis* proteins), activity buffer SA (for *S. aureus* proteins), or activity buffer CD (for CD spectroscopy control assays) in the presence of either low (1.5 μM ClpP; 1.5 μM ADEP) or high (1.5 μM ClpP; 3.75 μM ADEP, or 2.5 μM ClpP; 6.25 μM ADEP) concentrations of ADEP2 and ClpP monomer as indicated. Samples were taken at indicated time points and were analyzed via SDS-PAGE and immunodetection techniques (64). Where appropriate, protein amounts were calculated from SDS-PAGE band intensities measured via densitometry using Image Lab software (Bio-Rad). For quantitative/comparative analyses, a standard curve was generated representing 1 μg, 2 μg, 3 μg, 4 μg, and 5 μg of the control protein BsFtsZ$_{1-382}$, which was loaded on the same SDS-PAGE

as the protein samples derived from degradation experiments. Remaining FtsZ protein amounts in the ADEP-treated samples were then compared and normalized to the respective DMSO control reaction which was set to 100%. The data were plotted using mean values collected from three different degradation experiments and SDS-PAGE analyses for each FtsZ variant, with corresponding standard deviations indicated by error bars.

Suc-LY-AMC and FITC-casein degradation assays. For the degradation of the fluorescent peptide substrate Suc-LY-AMC, concentrations of ADEP2 and ClpP (monomer) were used as indicated. Peptidase assays were performed in activity buffer BS using 1.5 μM of purified ClpP protein and 400 μM of Suc-LY-AMC (dissolved in DMSO) in 100-μl reaction volumes. For the degradation of the fluorogenic protein fluorescein isothiocyanate-casein (FITC-casein; Sigma), concentrations of ADEP2 and ClpP (monomer) were used as indicated. Protease assays were performed in activity buffer BS using 1.5 μM of purified ClpP protein and 20 μM FITC-casein in 100-μl reaction volumes. In both peptidase and protease assays, an equal volume of DMSO compared to ADEP was used as a control. Corresponding DMSO samples were used as the baseline control and were subtracted from ADEP values. Hydrolysis of the peptide or protein substrates (indicated by fluorescence emission) was monitored in black, flat-bottom 96-well microplates (Sarstedt) at 37°C via measuring the release of either AMC or FITC, respectively, in a spectrofluorometer (Tecan Infinite M200) at an excitation wavelength (λex) of 380 nm and an emission wavelength (λem) of 460 nm (for Suc-LY-AMC) or at an λex of 490 nm and an λem of 525 nm (for FITC-casein).

Immunoblotting of FtsZ, GFP, and FbaA. To analyze the degradation of GFP-fused FtsZ in whole cells, *B. subtilis* strains 2014 and 2020 were cultivated in LB medium containing 1 mM isopropyl-β-D-thiogalactopyranoside (IPTG) and 0.5% xylose. Degradation of FtsZ and FbaA was further investigated using *B. subtilis* strain 168 as well as *S. aureus* strain NCTC 8325. Overnight cultures of all strains were diluted 1:200 in fresh LB (with or without appropriate inducers) and grown to an optical density at 600 nm (OD$_{600}$) of 0.1 to 0.25 at 37°C while shaking. Then, cultures were split, adding either ADEP2 or DMSO as a negative control. For *B. subtilis* strains 2014 and 2020, 0.5 μg/ml ADEP2 was used. For *B. subtilis* 168 and *S. aureus* NCTC 8325, 0.25 μg/ml or 3 μg/ml and 1 μg/ml or 8 μg/ml ADEP2 were used for low or high concentrations, respectively. Cultures were further shaken at 37°C for 60 or 120 minutes (as indicated). Cells were then harvested, suspended in 0.5 to 1 ml lysis buffer (50 mM NaH$_2$PO$_4$ and 300 mM NaCl [pH 8], with added EDTA-free mini protease inhibitor; Roche), and lysed via cell disruption in a PreCellys homogenizer (6,800 rpm, 3 times for 20 s) using a mixture of 0.1-μm and 0.5-μm glass beads in 0.5-ml PreCellys tubes. The protein content of the cell lysates was measured by Nanodrop spectrophotometry and adjusted accordingly. Immunoblotting of whole-cell extracts or purified proteins was performed by standard techniques (64) using anti-FtsZ, anti-GFP, anti-His$_6$, anti-FbaA, or anti-Div4A antibodies as indicated. A Coomassie blue-stained SDS-PAGE was additionally used to control the applied protein amount.

Protein identification by mass spectrometry. For orienting analyses, a partially truncated FtsZ protein was analyzed by label-free mass spectrometry (MS) using a Synapt G2-S HDMS time of flight (TOF) mass spectrometer equipped with an ESI NanoLockSpray source coupled online to a nanoAcquity ultraperformance liquid chromatography (UPLC) system and operated with MassLynx software (version V4.1 SCN932; Waters). Proteins were excised from the gel and destained twice in washing solution (20 mM ammonium bicarbonate, 30% acetonitrile). For reduction of disulfide bonds, gel pieces were incubated with 10 mM DTT in washing solution at 60°C for 45 min. Alkylation of cysteines was then performed with 50 mM iodoacetamide (IAA) in washing solution for 25 min at room temperature in the dark. Gel pieces were washed again twice with washing solution for 5 min at room temperature and dried using a vacuum centrifuge at 40°C prior to tryptic digestion with 6.25 ng/μl trypsin (Promega) in washing solution for 16 h at 37°C. Tryptic peptides were eluted using 20 μl of 0.1% trifluoroacetic acid and an ultrasonic bath for 15 min. Tryptic peptides were purified using a nanoAcquity UPLC trap symmetry C$_{18}$ column (pore size, 100 Å; particle size, 5 μm; length, 20 mm; Waters) with a flow of 10 μl/min in 0.5% buffer B for 4 min. Tryptic peptides were then eluted from a nanoAcquity UPLC CSH130 C$_{18}$ column (pore size, 130 Å; particle size, 1.7 μm; length, 100 mm; Waters) with a flow of 0.35 μl/min at 40°C using the following gradient: initial, 0.5% eluent B; 22 min, 60% eluent B; 24 min, 90% eluent B; 26 min, 99% eluent B; 27 min, 0.5% eluent B; and 30 min, 0.5% eluent B. Continuous MS^E spectra were recorded in a mass range from 50 to 1800 *m/z* and with a scan time of 1 s in positive resolution mode with the following settings: capillary voltage, 2.1 kV; cone voltage, 30 V; source temperature, 100°C; cone gas flow, 50 liters/h; desolvation gas flow, 550 liters/h; and desolvation temperature, 150°C. Collision energy was ramped from 14 to 45 eV. Serving as mass reference, leucine-encephalin was injected with a capillary voltage of 3 kV every 60 s. The mass spectra were processed with ProteinLynx Global Server (version 2.5.2; Waters). Processing parameters were adjusted as follows: chromatographic peak width, automatic; MS TOF resolution, automatic; lock mass for charge 1, 556.2771 Da/e; lock mass window, 0.25 Da; low energy threshold, 2,000 counts; elevated energy threshold, 500 counts; and intensity threshold, 10,000 counts. For protein identification, a data bank containing 4,156 proteins of *E. coli* BL21 (Uniprot reference sequence UP000002032, added manually; *B. subtilis* FtsZ and ClpP, trypsin, and keratin) was used. The following settings were used: peptide tolerance, automatic; fragment tolerance, automatic; min fragment ion matches per peptide, 5; min fragment ion matches per protein, 5; min peptide matches per protein, 1; maximum protein mass, 400,000; primary digest reagent, trypsin; secondary digest reagent, none; missed cleavages, 1; fixed modifications, carbamidomethyl C; variable modifications, deamidation N, deamidation Q, oxidation M; and false-positive rate, 4.

Edman protein sequencing. Edman protein sequencing was used to further characterize early fragments of native FtsZ degradation. To this end, 5 μM FtsZ protein was digested by ADEP2-ClpP as

described above and subsequently separated by SDS-PAGE (12%), followed by semidry electroblotting on a polyvinylidene difluoride (PVDF) membrane (blot buffer was 50 mM sodium borate [pH 9.0], 0.1% SDS, and 20% methanol) for 4 h at 4°C. Transferred proteins were stained with Ponceau S solution (0.5% Ponceau S and 1% acetic acid in deionized water) for 6 min, and desired bands were excised. Automated Edman protein sequencing was performed by Genaxxon (Germany) using a Procise capillary-liquid chromatography (cLC) Edman sequencer (Applied Biosystems), including N-terminal degradation steps 1 to 5 with amino acid identification and verification.

SUPPLEMENTAL MATERIAL

Supplemental material is available online only.

FIG S1, PDF file, 0.6 MB.
FIG S2, PDF file, 0.05 MB.
FIG S3, PDF file, 0.7 MB.
FIG S4, PDF file, 0.2 MB.
FIG S5, PDF file, 2.1 MB.
FIG S6, PDF file, 1 MB.
FIG S7, PDF file, 0.5 MB.
FIG S8, PDF file, 0.3 MB.
TABLE S1, PDF file, 0.1 MB.
TABLE S2, PDF file, 0.04 MB.

REFERENCES

1. Brötz-Oesterhelt H, Beyer D, Kroll HP, Endermann R, Ladel C, Schroeder W, Hinzen B, Raddatz S, Paulsen H, Henninger K, Bandow JE, Sahl HG, Labischinski H. 2005. Dysregulation of bacterial proteolytic machinery by a new class of antibiotics. Nat Med 11:1082–1087. https://doi.org/10.1038/nm1306.

2. Brown Gandt A, Griffith EC, Lister IM, Billings LL, Han A, Tangallapally R, Zhao Y, Singh AP, Lee RE, LaFleur MD. 2018. In vivo and in vitro effects of a ClpP-activating antibiotic against vancomycin-resistant enterococci. Antimicrob Agents Chemother 62:e00424-18. https://doi.org/10.1128/AAC.00424-18.

3. Conlon BP, Nakayasu ES, Fleck LE, LaFleur MD, Isabella VM, Coleman K, Leonard SN, Smith RD, Adkins JN, Lewis K. 2013. Activated ClpP kills persisters and eradicates a chronic biofilm infection. Nature 503:365–370. https://doi.org/10.1038/nature12790.

4. Thomy D, Culp E, Adamek M, Cheng EY, Ziemert N, Wright GD, Sass P, Brötz-Oesterhelt H. 2019. The ADEP biosynthetic gene cluster in Streptomyces hawaiiensis NRRL 15010 reveals an accessory clpP gene as a novel antibiotic resistance factor. Appl Environ Microbiol 85:e01292-19. https://doi.org/10.1128/AEM.01292-19.

5. Bukau B, Weissman J, Horwich A. 2006. Molecular chaperones and protein quality control. Cell 125:443–451. https://doi.org/10.1016/j.cell.2006.04.014.

6. Frees D, Gerth U, Ingmer H. 2014. Clp chaperones and proteases are central in stress survival, virulence and antibiotic resistance of Staphylococcus aureus. Int J Med Microbiol 304:142–149. https://doi.org/10.1016/j.ijmm.2013.11.009.

7. Brötz-Oesterhelt H, Sass P. 2014. Bacterial caseinolytic proteases as novel targets for antibacterial treatment. Int J Med Microbiol 304:23–30. https://doi.org/10.1016/j.ijmm.2013.09.001.

8. Baker TA, Sauer RT. 2012. ClpXP, an ATP-powered unfolding and protein-degradation machine. Biochim Biophys Acta 1823:15–28. https://doi.org/10.1016/j.bbamcr.2011.06.007.

9. Raju RM, Goldberg AL, Rubin EJ. 2012. Bacterial proteolytic complexes as therapeutic targets. Nat Rev Drug Discov 11:777–789. https://doi.org/10.1038/nrd3846.

10. Kirstein J, Moliere N, Dougan DA, Turgay K. 2009. Adapting the machine: adaptor proteins for Hsp100/Clp and AAA+ proteases. Nat Rev Microbiol 7:589–599. https://doi.org/10.1038/nrmicro2185.

11. Kim YI, Levchenko I, Fraczkowska K, Woodruff RV, Sauer RT, Baker TA. 2001. Molecular determinants of complex formation between Clp/Hsp100 ATPases and the ClpP peptidase. Nat Struct Biol 8:230–233. https://doi.org/10.1038/84967.

12. Olivares AO, Baker TA, Sauer RT. 2016. Mechanistic insights into bacterial AAA+ proteases and protein-remodelling machines. Nat Rev Microbiol 14:33–44. https://doi.org/10.1038/nrmicro2015.4.

13. Kirstein J, Hoffmann A, Lilie H, Schmidt R, Rübsamen-Waigmann H,

Brötz-Oesterhelt H, Mogk A, Turgay K. 2009. The antibiotic ADEP reprogrammes ClpP, switching it from a regulated to an uncontrolled protease. EMBO Mol Med 1:37–49. https://doi.org/10.1002/emmm .200900002.

14. Famulla K, Sass P, Malik I, Akopian T, Kandror O, Alber M, Hinzen B, Ruebsamen-Schaeff H, Kalscheuer R, Goldberg AL, Brötz-Oesterhelt H. 2016. Acyldepsipeptide antibiotics kill mycobacteria by preventing the physiological functions of the ClpP1P2 protease. Mol Microbiol 101: 194–209. https://doi.org/10.1111/mmi.13362.

15. Leodolter J, Warweg J, Weber-Ban E. 2015. The *Mycobacterium tuberculosis* ClpP1P2 protease interacts asymmetrically with its ATPase partners ClpX and ClpC1. PLoS One 10:e0125345. https://doi.org/10.1371/journal .pone.0125345.

16. Raju RM, Unnikrishnan M, Rubin DH, Krishnamoorthy V, Kandror O, Akopian TN, Goldberg AL, Rubin EJ. 2012. *Mycobacterium tuberculosis* ClpP1 and ClpP2 function together in protein degradation and are required for viability *in vitro* and during infection. PLoS Pathog 8:e1002511. https://doi.org/10.1371/journal.ppat.1002511.

17. Gersch M, Famulla K, Dahmen M, Göbl C, Malik I, Richter K, Korotkov VS, Sass P, Rübsamen-Schaeff H, Madl T, Brötz-Oesterhelt H, Sieber SA. 2015. AAA+ chaperones and acyldepsipeptides activate the ClpP protease via conformational control. Nat Commun 6:6320. https://doi.org/10.1038/ ncomms7320.

18. Malik IT, Brötz-Oesterhelt H. 2017. Conformational control of the bacterial Clp protease by natural product antibiotics. Nat Prod Rep 34: 815–831. https://doi.org/10.1039/c6np00125d.

19. Lee B-G, Park EY, Lee K-E, Jeon H, Sung KH, Paulsen H, Rübsamen-Schaeff H, Brötz-Oesterhelt H, Song HK. 2010. Structures of ClpP in complex with a novel class of antibiotics reveal its activation mechanism. Nat Struct Mol Biol 17:471–478. https://doi.org/10.1038/nsmb.1787.

20. Li DH, Chung YS, Gloyd M, Joseph E, Ghirlando R, Wright GD, Cheng YQ, Maurizi MR, Guarne A, Ortega J. 2010. Acyldepsipeptide antibiotics induce the formation of a structured axial channel in ClpP: a model for the ClpX/ClpA-bound state of ClpP. Chem Biol 17:959–969. https://doi .org/10.1016/j.chembiol.2010.07.008.

21. Malik IT, Pereira R, Vielberg MT, Mayer C, Straetener J, Thomy D, Famulla K, Castro H, Sass P, Groll M, Brötz-Oesterhelt H. 2020. Functional characterisation of ClpP mutations conferring resistance to acyldepsipeptide antibiotics in Firmicutes. Chembiochem https://doi.org/10.1002/cbic .201900787.

22. Sass P, Josten M, Famulla K, Schiffer G, Sahl HG, Hamoen L, Brötz-Oesterhelt H. 2011. Antibiotic acyldepsipeptides activate ClpP peptidase to degrade the cell division protein FtsZ. Proc Natl Acad Sci U S A 108:17474–17479. https://doi.org/10.1073/pnas.1110385108.

23. Mayer C, Sass P, Brötz-Oesterhelt H. 2019. Consequences of dosing and timing on the antibacterial effects of ADEP antibiotics. Int J Med Microbiol 309:151329. https://doi.org/10.1016/j.ijmm.2019.151329:151329.

24. Oliva MA, Cordell SC, Löwe J. 2004. Structural insights into FtsZ protofilament formation. Nat Struct Mol Biol 11:1243–1250. https://doi.org/10 .1038/nsmb855.

25. Löwe J, Amos LA. 1998. Crystal structure of the bacterial cell-division protein FtsZ. Nature 391:203–206. https://doi.org/10.1038/34472.

26. Nogales E, Downing KH, Amos LA, Löwe J. 1998. Tubulin and FtsZ form a distinct family of GTPases. Nat Struct Biol 5:451–458. https://doi.org/ 10.1038/nsb0698-451.

27. Scheffers DJ, de Wit JG, den Blaauwen T, Driessen AJ. 2002. GTP hydrolysis of cell division protein FtsZ: evidence that the active site is formed by the association of monomers. Biochemistry 41:521–529. https://doi .org/10.1021/bi011370i.

28. Flynn JM, Levchenko I, Seidel M, Wickner SH, Sauer RT, Baker TA. 2001. Overlapping recognition determinants within the ssrA degradation tag allow modulation of proteolysis. Proc Natl Acad Sci U S A 98: 10584–10589. https://doi.org/10.1073/pnas.191375298.

29. Mukherjee A, Lutkenhaus J. 1998. Dynamic assembly of FtsZ regulated by GTP hydrolysis. EMBO J 17:462–469. https://doi.org/10.1093/emboj/ 17.2.462.

30. Erickson HP, Anderson DE, Osawa M. 2010. FtsZ in bacterial cytokinesis: cytoskeleton and force generator all in one. Microbiol Mol Biol Rev 74:504–528. https://doi.org/10.1128/MMBR.00021-10.

31. Adams DW, Errington J. 2009. Bacterial cell division: assembly, maintenance and disassembly of the Z-ring. Nat Rev Microbiol 7:642–653. https://doi.org/10.1038/nrmicro2198.

32. Sundararajan K, Goley ED. 2017. The intrinsically disordered C-terminal linker of FtsZ regulates protofilament dynamics and superstructure in

vitro. J Biol Chem 292:20509–20527. https://doi.org/10.1074/jbc.M117 .809939.

33. Scheffers DJ, Driessen AJ. 2002. Immediate GTP hydrolysis upon FtsZ polymerization. Mol Microbiol 43:1517–1521. https://doi.org/10.1046/j .1365-2958.2002.02828.x.

34. Huecas S, Andreu JM. 2004. Polymerization of nucleotide-free, GDP- and GTP-bound cell division protein FtsZ: GDP makes the difference. FEBS Lett 569:43–48. https://doi.org/10.1016/j.febslet.2004.05.048.

35. Romberg L, Simon M, Erickson HP. 2001. Polymerization of Ftsz, a bacterial homolog of tubulin. Is assembly cooperative? J Biol Chem 276:11743–11753. https://doi.org/10.1074/jbc.M009033200.

36. Hsin J, Gopinathan A, Huang KC. 2012. Nucleotide-dependent conformations of FtsZ dimers and force generation observed through molecular dynamics simulations. Proc Natl Acad Sci U S A 109:9432–9437. https://doi.org/10.1073/pnas.1120761109.

37. Raymond A, Lovell S, Lorimer D, Walchli J, Mixon M, Wallace E, Thompkins K, Archer K, Burgin A, Stewart L. 2009. Combined protein construct and synthetic gene engineering for heterologous protein expression and crystallization using Gene Composer. BMC Biotechnol 9:37. https:// doi.org/10.1186/1472-6750-9-37.

38. Mukherjee A, Lutkenhaus J. 1999. Analysis of FtsZ assembly by light scattering and determination of the role of divalent metal cations. J Bacteriol 181:823–832. https://doi.org/10.1128/JB.181.3.823-832.1999.

39. Bramhill D, Thompson CM. 1994. GTP-dependent polymerization of *Escherichia coli* FtsZ protein to form tubules. Proc Natl Acad Sci U S A 91:5813–5817. https://doi.org/10.1073/pnas.91.13.5813.

40. Yu XC, Margolin W. 1997. Ca2+-mediated GTP-dependent dynamic assembly of bacterial cell division protein FtsZ into asters and polymer networks in vitro. EMBO J 16:5455–5463. https://doi.org/10.1093/emboj/ 16.17.5455.

41. Scheffers DJ, den Blaauwen T, Driessen AJ. 2000. Non-hydrolysable GTP-gamma-S stabilizes the FtsZ polymer in a GDP-bound state. Mol Microbiol 35:1211–1219. https://doi.org/10.1046/j.1365-2958.2000.01791.x.

42. Li Y, Hsin J, Zhao L, Cheng Y, Shang W, Huang KC, Wang HW, Ye S. 2013. FtsZ protofilaments use a hinge-opening mechanism for constrictive force generation. Science 341:392–395. https://doi.org/10.1126/science .1239248.

43. Pauling L, Corey RB, Branson HR. 1951. The structure of proteins; two hydrogen-bonded helical configurations of the polypeptide chain. Proc Natl Acad Sci U S A 37:205–211. https://doi.org/10.1073/pnas.37.4.205.

44. Eisenberg D. 2003. The discovery of the alpha-helix and beta-sheet, the principal structural features of proteins. Proc Natl Acad Sci U S A 100:11207–11210. https://doi.org/10.1073/pnas.2034522100.

45. Camberg JL, Hoskins JR, Wickner S. 2009. ClpXP protease degrades the cytoskeletal protein, FtsZ, and modulates FtsZ polymer dynamics. Proc Natl Acad Sci U S A 106:10614–10619. https://doi.org/10.1073/pnas .0904886106.

46. Camberg JL, Viola MG, Rea L, Hoskins JR, Wickner S. 2014. Location of dual sites in *E. coli* FtsZ important for degradation by ClpXP; one at the C-terminus and one in the disordered linker. PLoS One 9:e94964. https:// doi.org/10.1371/journal.pone.0094964.

47. Weart RB, Nakano S, Lane BE, Zuber P, Levin PA. 2005. The ClpX chaperone modulates assembly of the tubulin-like protein FtsZ. Mol Microbiol 57: 238–249. https://doi.org/10.1111/j.1365-2958.2005.04673.x.

48. Haeusser DP, Lee AH, Weart RB, Levin PA. 2009. ClpX inhibits FtsZ assembly in a manner that does not require its ATP hydrolysis-dependent chaperone activity. J Bacteriol 191:1986–1991. https://doi .org/10.1128/JB.01606-07.

49. Andreu JM, Oliva MA, Monasterio O. 2002. Reversible unfolding of FtsZ cell division proteins from archaea and bacteria. Comparison with eukaryotic tubulin folding and assembly. J Biol Chem 277:43262–43270. https://doi.org/10.1074/jbc.M206723200.

50. Diaz-Espinoza R, Garces AP, Arbildua JJ, Montecinos F, Brunet JE, Lagos R, Monasterio O. 2007. Domain folding and flexibility of *Escherichia coli* FtsZ determined by tryptophan site-directed mutagenesis. Protein Sci 16:1543–1556. https://doi.org/10.1110/ps.072807607.

51. Santra MK, Panda D. 2003. Detection of an intermediate during unfolding of bacterial cell division protein FtsZ: loss of functional properties precedes the global unfolding of FtsZ. J Biol Chem 278:21336–21343. https://doi.org/10.1074/jbc.M301303200.

52. Montecinos-Franjola F, Ross JA, Sanchez SA, Brunet JE, Lagos R, Jameson DM, Monasterio O. 2012. Studies on the dissociation and urea-induced unfolding of FtsZ support the dimer nucleus polymerization mechanism. Biophys J 102:2176–2185. https://doi.org/10.1016/j.bpj.2012.03.064.

53. Huecas S, Canosa-Valls AJ, Araújo-Bazán L, Ruiz FM, Laurents DV, Fernández-Tornero C, Andreu JM. 2020. Nucleotide-induced folding of cell division protein FtsZ from Staphylococcus aureus. FEBS J https://doi .org/10.1111/febs.15235.

54. Sowole MA, Alexopoulos JA, Cheng YQ, Ortega J, Konermann L. 2013. Activation of ClpP protease by ADEP antibiotics: insights from hydrogen exchange mass spectrometry. J Mol Biol 425:4508–4519. https://doi.org/ 10.1016/j.jmb.2013.08.005.

55. Wang J, Hartling JA, Flanagan JM. 1997. The structure of ClpP at 2.3 A resolution suggests a model for ATP-dependent proteolysis. Cell 91: 447–456. https://doi.org/10.1016/S0092-8674(00)80431-6.

56. Garcia-Seisdedos H, Empereur-Mot C, Elad N, Levy ED. 2017. Proteins evolve on the edge of supramolecular self-assembly. Nature 548: 244–247. https://doi.org/10.1038/nature23320.

57. Wong KS, Mabanglo MF, Seraphim TV, Mollica A, Mao YQ, Rizzolo K, Leung E, Moutaoufik MT, Hoell L, Phanse S, Goodreid J, Barbosa LRS, Ramos CHI, Babu M, Mennella V, Batey RA, Schimmer AD, Houry WA. 2018. Acyldepsipeptide analogs dysregulate human mitochondrial ClpP protease activity and cause apoptotic cell death. Cell Chem Biol 25: 1017–1030.e9. https://doi.org/10.1016/j.chembiol.2018.05.014.

58. Schmitz KR, Carney DW, Sello JK, Sauer RT. 2014. Crystal structure of Mycobacterium tuberculosis ClpP1P2 suggests a model for peptidase activation by AAA+ partner binding and substrate delivery. Proc Natl Acad Sci U S A 111:E4587–E4595. https://doi.org/10.1073/pnas.1417120111.

59. Huecas S, Llorca O, Boskovic J, Martin-Benito J, Valpuesta JM, Andreu JM. 2008. Energetics and geometry of FtsZ polymers: nucleated self-assembly of single protofilaments. Biophys J 94:1796–1806. https://doi .org/10.1529/biophysj.107.115493.

60. Buske PJ, Levin PA. 2013. A flexible C-terminal linker is required for proper FtsZ assembly in vitro and cytokinetic ring formation in vivo. Mol Microbiol 89:249–263. https://doi.org/10.1111/mmi.12272.

61. Wang X, Lutkenhaus J. 1993. The FtsZ protein of Bacillus subtilis is localized at the division site and has GTPase activity that is dependent upon FtsZ concentration. Mol Microbiol 9:435–442. https://doi.org/10 .1111/j.1365-2958.1993.tb01705.x.

62. Sass P, Bierbaum G. 2007. Lytic activity of recombinant bacteriophage phi11 and phi12 endolysins on whole cells and biofilms of Staphylococcus aureus. Appl Environ Microbiol 73:347–352. https://doi.org/10.1128/ AEM.01616-06.

63. Krol E, Scheffers DJ. 2013. FtsZ polymerization assays: simple protocols and considerations. J Vis Exp e50844. https://doi.org/10.3791/50844.

64. Sambrook J, Fritsch EF, Maniatis T. 1989. Molecular cloning: a laboratory manual, 2nd edition. Cold Spring Harbor Laboratory Press, Cold Spring Harbor, NY.

65. Pereira SF, Gonzalez RL, Jr, Dworkin J. 2015. Protein synthesis during cellular quiescence is inhibited by phosphorylation of a translational elongation factor. Proc Natl Acad Sci U S A 112:E3274–E3281. https:// doi.org/10.1073/pnas.1505297112.

66. Yang ZR, Thomson R, McNeil P, Esnouf RM. 2005. RONN: the bio-basis function neural network technique applied to the detection of natively disordered regions in proteins. Bioinformatics 21:3369–3376. https://doi .org/10.1093/bioinformatics/bti534.

67. Kyte J, Doolittle RF. 1982. A simple method for displaying the hydropathic character of a protein. J Mol Biol 157:105–132. https://doi.org/10 .1016/0022-2836(82)90515-0.